# Mineralogical and spectral (NIR) characterization of Fe-rich vermiculite-bearing terrestrial deposits and constraints for mineralogy of Oxia Planum, ExoMars 2022 landing site.

Agata M. Krzesińska[a,] *, Benjamin Bultel[a], Damien Loizeau[b], David Craw[c], Richard April[d], François Poulet[b], Stephanie C. Werner[a]

[a] Centre for Earth Evolution and Dynamics (CEED), Department of Geosciences, University of Oslo, Postboks 1028 Blindern, 0316 Oslo, Norway Oslo, Norway
[b] Institut d'Astrophysique Spatiale, Université Paris-Sud, 91400 Orsay, France
[c]Geology Department, University of Otago, PO Box 56, Dunedin 9054, New Zealand.
[d]Geology Department, Colgate University, Hamilton, NY 13346, USA
*corresponding authors: a.m.krzesinska@geo.uio.no; benjamin.bultel@geo.uio.no

## Abstract:

Oxia Planum is a Noachian plain on Mars. It was chosen as the final landing site for in-situ studies by ExoMars 2022 rover. Main scientific objectives of the mission are to understand the mineralogy and aqueous evolution of ancient Mars with relevance to habitability. Oxia is covered by vast deposits of Fe,Mg-phyllosilicates, but the exact nature of these deposits is not yet fully understood. We performed a survey of potential terrestrial analogue rocks and here we show combined mineralogical characterization of these rocks with their NIR spectral analysis. Samples from two terrestrial sites were studied: 1) vermiculitized chlorite-schists from Otago, New Zealand, which underwent an alteration process without significant oxidation; and 2) basaltic tuffs from Granby, Massachusetts, USA, with Fe-rich clays filling amygdales of supposedly hydrothermal origin. Both analogues are incorporated into the newly built Planetary Terrestrial Analogue Library (PTAL) collection.

Oxia bedrock clay-rich deposits are spectrally matched best by a well crystallized trioctahedral vermiculite-saponite mixture from the basaltic tuff, although the contribution of saponite must be minor.

Otago vermiculite is a good analogue to Oxia vermiculite in terms of overall mineralogy and Fe content. However, spectral inconsistencies related to the Al content in the Otago clays indicate that illitization of vermiculite, which results from post-alteration oxidation, did not occur at Oxia. This implies limited water-rock interactions and reducing conditions during deposition of sediments now constituting the bedrock at Oxia.

Whereas the spectral match does not conclusively imply the mineralogy, trioctahedral vermiculite should be considered as a likely mineral component of the bedrock unit at Oxia

Planum. Vermiculite has great potential to store organic matter and the post-deposition geological context of Oxia Planum derived from understanding of environmental conditions in analogue sites is promising for organic matter preservation.

## 1. Introduction

In 2022, the European Space Agency (ESA) in cooperation with the Russian State Corporation for Space Activities (Roscosmos) will launch the ExoMars mission to land rover Rosalind Franklin on Mars. Oxia Planum, a wide, low-lying plain located at the Martian dichotomy on the margins of the Chryse Planitia basin, between Mawrth and Ares Valles was selected as the final landing site for the rover. Geomorphological features of this plain and mineral exposures interpreted to be clay minerals (phyllosilicates) at the site indicate an old and complex history of aqueous alteration (Quantin-Nataf et al., 2020). The minerals present in the landing site region suggest an environment that supports (if not favours) accumulation and preservation of organic matter (Farmer and Des Marais, 1999). Therefore, in-situ studies of Oxia Planum are expected to answer scientific questions posed by the ExoMars 2022 mission pertaining to the history of water and the geochemical environment in the shallow Martian subsurface, and address the ancient and present habitability of the planet (Vago et al., 2017; Quantin-Nataf et al., 2020).

Remote sensing observations were used to choose a landing ellipse (~19 x 120 km) comprising 70% of middle- to late-Noachian (>3.9 Ga) in age, stratified bedrock deposits rich in hydrous Fe,Mg-clays (Carter et al., 2016, Turner and Bridges, 2017, Quantin-Nataf et al., 2020, Mandon et al., 2021). The bedrock unit is one of the largest exposures of this type on Mars and is more than 50 m thick (Quantin-Nataf et al., 2020), although the exact amount of clays in this region is not fully recognized from the orbit. The origin of such voluminous Fe,Mg-phyllosilicates deposits is not yet fully understood. Layering within the deposits reported by Mandon et al. (2021), and draping of the topography documented by Quantin-Nataf et al. (2020) suggest that the bedrock phyllosilicates formed either in a subaqueous environment (palustrine, lacustrine or marine), or either in subaerial conditions compatible with airborne volcaniclastics altered by pedogenesis, or via aeolian deposits. Furthermore, geomorphological features indicate that postdating deposition of the bedrock unit, a separate aqueous event occurred in this place, most likely connected to fluvial and deltaic activity (Turner and Bridges, 2017; Quantin-Nataf et al., 2020). Understanding of environmental conditions and processes involved in the formation of the bedrock unit could be enhanced by better characterizing the mineralogy of the deposits. The exact identification of Fe,Mg-phyllosilicates remains uncertain, however.

In order to better prepare for scientific return of the ExoMars 2022 rover mission, understanding the mineralogical nature of bedrock deposits related to aqueous events is desired as this may hold clues for both habitability potential and biosignature preservation. Before landing, studies of terrestrial analogue sites provide promising approach to evaluate potential formation scenarios of bedrock, which can be verified by the measurements of onboard instruments of the Rosalind Franklin rover.

In this report, we present a survey of terrestrial rocks that are potential spectral analogues to Oxia Planum bedrock deposits. We characterize their mineralogy, reconstruct the aqueous conditions during their formation and by this, provide constraints for water-rock interactions at Oxia Planum to assess the biosignature preservation potential. Although the spectral analogy never implies exact parallelism in processes of deposit formation, identification of specific minerals can shed light on recorded alterations, making some processes likely or unlikely. The collected analogues have been added to the Planetary Terrestrial Analogue Library collection (www.ptal.eu), which is built with the overarching goal of providing the scientific community with terrestrial analogue rocks that support interpretation of in-situ Martian missions (Dypvik et al., in review PSS).

## 2. NIR characterization of bedrock deposits at Oxia

Oxia Planum bedrock deposits, when characterized in the near infrared by CRISM (*Compact Reconnaissance Imaging Spectrometer for Mars*) and OMEGA (*Observatoire pour la Minéralogie, l'Eau, les Glaces et l'Activité*) instruments, exhibit signals of a large and deep absorption near 1.00 µm, creating a positive slope from ~1.0 µm to ~1.8 µm, a small V-shaped absorption near 1.41–1.44 µm, a large and deep V-shaped absorption near 1.92 µm, a deep absorption near 2.31–2.32 µm, a weak absorption near 2.38-2.41 µm (which sometimes is manifested only as change of slope) and a large and deep absorption near 2.90-2.95 µm (Table 1). The continuum of the spectrum is influenced mainly by the three absorptions near 1.00 µm, 2.30 µm and 2.90 µm (Fig. 1). A weak absorption near 2.20 µm is possibly observed by OMEGA, but is not confidently identified with CRISM and a band is sometimes present near 2.5 µm. The latter have been attributed to a possible additional mineral locally present at the site.

Attribution of specific absorptions to electronic transition, stretching and bending-related vibrations enables interpretation of a NIR spectrum and can provide information on mineral composition and the nature of the phyllosilicate material (Table 1). Based on the above attribution of absorptions, spectral features of Oxia bedrock clay deposits suggest the presence

of Fe,Mg-rich phyllosilicates with significant amounts of $Fe^{2+}$ in octahedral sites (i.e., the phyllosilicates are mostly trioctahedral). The position of the band near 1.00 µm and 1.41–1.42 µm suggests an $Fe^{2+}$-rich clay component; the position and shoulder slope of the band near 2.30 µm, together with the 2.39 µm band suggest mainly a trioctahedral nature of clays ($Fe^{2+}$ and $Mg^{2+}$); and an occasional weak band near 2.20–2.23 µm (Al and Al + $Fe^{3+}$) would indicate that a dioctahedral component may co-exist. Together with the plateau-shaped absorption near 2.30 µm linked to a complex mixture of Fe,Mg-OH, it can be inferred that bedrock deposits at Oxia Planum consist of mixed-layer clay minerals rich in Fe and Mg, but the presence of Al is disputable. The spectral features are consistent with either smectite clays ($Fe^{2+}$-rich saponite), or vermiculite (Carter et al., 2016). Mica or interstratified mica and vermiculite are also possible. Carter et al. (2016) considered vermiculite the better interpretation, despite library spectra of vermiculite currently available that do not provide a perfect match for the phyllosilicates tentatively identified at Oxia Planum (Fig. 1). Therefore, we set out to find the best terrestrial spectral analogue material, which provides the main characteristics of the Oxia Planum bedrock deposits, namely natural terrestrial Fe-rich, trioctahedral vermiculite.

## 3. Survey of best terrestrial analogues with vermiculite-like minerals

Lack of full consistency between the NIR library spectra of terrestrial vermiculite and NIR spectra of Oxia bedrock clay deposits may be the result of monomineralic terrestrial (or synthetic) standards used as a comparison. In such cases, overlapping vibrational absorption features of mixed mineral phases of natural rocks are missing. Therefore, it can be challenging to compare library and natural rock spectra. This cannot be assessed in a simple way. To overcome this issue, spectra of natural terrestrial rocks, potentially best matching the original exposures, should be used for comparison (e.g., Veneranda et al., 2019; Lantz et al., 2020; Dypvik et al., in review). Imperfect spectral matches can also result from the variable chemical and physical nature of natural vermiculite, which often occurs interstratified with chlorite, illite and smectite, the effects of which on spectral appearance is not fully understood (Campos et al., 2009).

In order to assess the spectral analogy of Oxia Planum phyllosilicates to natural vermiculite-bearing rocks, we have identified terrestrial deposits of Fe-rich, trioctahedral vermiculite, and in this paper we present their mineralogical description and NIR spectral characterization.

Based on NIR spectra of Oxia Planum bedrock phyllosilicates, our search for the best terrestrial analogues focused on the following requirements: (1) vermiculite must be mainly trioctahedral, which implies minor Al in octahedral sites and minimal oxidation of octahedral

Fe; (2) vermiculite occurs as a mixed-layer clay, some minor substitution of Al may exist in its structure; and (3) vermiculite is $Fe^{2+}$-rich as opposed to $Fe^{3+}$-rich.

### 3.1. Vermiculite structural types and formation pathways

Vermiculite is a mica-type phyllosilicate with a 2:1, TOT structure. Vermiculite can occur in two main structural types (Fig. 2): (1) dioctahedral, aluminuous vermiculite with two $Al^{3+}$ cations dominating in octahedral sites and tetrahedral $Si^{4+}$ partially replaced by $Al^{3+}$; and (2) trioctahedral, siliceous vermiculite in which three $Fe^{2+}$ and $Mg^{2+}$ occupy octahedral sites and tetrahedral positions are occupied almost exclusively by $Si^{4+}$. Further complexities in the structure, however, may occur when octahedral iron is oxidized causing expulsion of octahedral cations to maintain charge balance and (partial) transformation of the structure from trioctahedral to dioctahedral (Fig. 2).

Vermiculite is an alteration product and both its chemistry and structure are inherited from the primary minerals from which it is derived. Vermiculite forms via alteration of micas such as muscovite, phlogopite-biotite-annite and chlorite (Fig. 2). Vermiculitization progresses mainly via removal of interlayer potassium ions from micas (Gordeeva et al., 2002) or by dissolution of the gibbsite-like or brucite-like layers from chlorite, and their replacement by $Mg^{2+}$ and water molecules in interlayer sites (Fig. 2, Wey and LeDred, 1972; Velde and Meunier, 2008). As such, vermiculitization of muscovite leads to the formation of dioctahedral, aluminous vermiculite, while vermiculitization of biotite and chlorite has the potential to form a trioctahedral, Fe,Mg-rich variety (Gordeeva et al., 2002). Alteration of biotite and chlorite in an oxidizing environment, however, may lead to formation of dioctahedral vermiculite via oxidation of octahedral $Fe^{2+}$ to $Fe^{3+}$ (Gilkes et al. 1972).

In the case of chlorite weathering, vermiculitization occurs through a series of mixed-layer minerals (Makubmi and Herbillon, 1972; Velde and Meunier, 2008). Typically, in terrestrial conditions, vermiculitization of chlorites is associated with oxidation of $Fe^{2+}$ cations in octahedral sites. The $Mg^{2+}$ cations are widely leached out from the octahedral and brucite-like sheets leading to relative enrichment in Si and Al (Ross and Kodama, 1976; Proust et al., 1986). Oxidation of octahedral $Fe^{2+}$ considerably changes the charge of the octahedral sheet and causes removal of Mg and/or Fe cations from site. This transforms the trioctahedral nature of the phyllosilicate to a dioctahedral one (Proust et al., 1986) and leads to the formation of a series of di- and tri- octahedral mixed layer minerals (Murakami et al., 1996).

Due to oxidative conditions prevailing during terrestrial weathering, most naturally occurring vermiculites have, in fact, a quite low $Fe^{2+}/Fe^{3+}$ ratio and therefore are mainly

dioctahedral (Newman and Brown, 1987). As such these vermiculites cannot serve as a good analogue for Oxia Planum bedrock deposits. However, as shown in laboratory experiments (Murakami et al., 2004; Sugimori et al., 2009), anoxic conditions during biotite or chlorite alteration can favour formation of $Fe^{2+}$-rich, trioctahedral vermiculite. Therefore, our search for possible vermiculite-bearing analogues for Oxia Planum bedrock deposits was designed to search for vermiculite that formed in environments that escaped extensive oxidation.

### 3.2. Terrestrial vermiculite deposits

In terrestrial conditions, vermiculite can be found in various geological environments that are relevant to supergene alteration of mica-bearing protolith rocks. Formation of vermiculite is generally attributed to low-temperature weathering processes (Basset, 1959; Fanning et al., 1989) but higher-temperature, hydrothermal conditions cannot be fully excluded from leading to vermiculitization (e.g., Ruiz Cruz, 1999), although debated (Basset, 1959).

The largest terrestrial vermiculite deposits are associated with altered Mg-rich phlogopite-bearing igneous or metamorphic rocks. These include worldwide deposits such as: Libby in Montana, USA (Basset 1959; Vam Gosen and Bush, 2001), Loolekoop, Phalaborwa, South Africa (Schoeman, 1989), or Kovdor massif, Kola Peninsula in Russia (Krasnova et al., 2004). Vermiculites in these locations are trioctahedral but have low Fe/Mg ratios, and, as such, are not expected to be good mineralogical matches for Oxia Planum.

As for our knowledge, and based on literature reviews of vermiculite deposits, Fe-rich vermiculite that formed under relatively anoxic conditions can be found in only two reported terrestrial localities. These are diagenetic clays in conglomerates formed in Otago schists, New Zealand (Craw et al., 1984; Craw et al. 1995; Kerr et al. 2017) and clay minerals filling amygdales in basaltic tuffs in the Granby Tuff, Connecticut, USA (April and Keller, 1992). The Otago clays formed after alteration of low-grade metamorphic chlorite (Craw et al., 1984) and clay in the Granby Tuff are of purportedly hydrothermal origin (April and Keller, 1992).

The main goal of this report is to identify the best spectral analogues to the phyllosilicates at Oxia. Mineralogical analogies identified will be discussed, as far as possible, to further our understanding of the environmental conditions under which the bedrock unit at Oxia formed. Despite the fact that the origin of primary minerals (i.e. biotite and chlorite as vermiculite precursors) in the terrestrial analogue environments may not necessary imply the same origin at Oxia Planum, we highlight that both hydrothermal and low-grade metamorphic conditions

(as those recorded in Otago and Granby rocks) likely occurred on Noachian Mars and led to the formation of chlorite (e.g., Ehlmann et al., 2011, Semprich et al., 2019).

### 3.2.1. Otago schist geological context

The Otago schists of southern New Zealand are greenschist-facies quartzo-feldspathic rocks (Bishop 1982; Mortensen et al., 2010) rich in Fe-rich chlorite, and phengitic muscovite, as well as low-grade metamorphic minerals such as pumpellyite actinolite, stilpnomelane and biotite (Brown, 1967; Malloch et al., 2017). Post-metamorphic uplift, mostly fault-controlled, has caused erosion under varying extensional and compressional tectonic regimes between Cretaceous and Holocene (Craw et al., 1995; Bishop and Turnbull, 1996, Els et al., 2002; Mortensen et al., 2010). Sediments containing schist clasts derived from fresh outcrops, locally deposited on unoxidized schist basement, have formed throughout this tectonic history (Craw 1984; Craw et al. 1995). Rapid dynamics of individual uplift events accompanied by protracted erosion time permitted deposition and retention of non-oxidizing or mild oxidative conditions (Craw et al., 1984). Additionally, the sediments contain variable amounts of organic matter that includes dispersed carbonaceous plant debris and some interbedded coal seams, which maintained a low redox state in the sediments. Diagenetic pyrite or marcasite is common, and at least some of the sulfides are biogenic (Tostevin et al. 2017).

Metamorphic chlorite remained unoxidized during erosion, transport and deposition in these deposits (Craw et al. 1995). However, diagenetic alteration of chlorite and associated muscovite has occurred as a result of interaction with groundwaters low in oxygen, causing transformation of the phyllosilicates to green $Fe^{2+}$-bearing clay minerals in a compositional series from vermiculite to kaolinite (Craw, 1984; Craw et al., 1995). This alteration occurred mainly via direct replacement. These clay minerals are interlayered with each other, and with primary minerals and are 10-20 µm in size. The least altered minerals in this series are trioctahedral, where octahedral sites are dominated by Mg and Fe with at least two-thirds of the latter being $Fe^{2+}$ (Craw 1984). Progressive alteration caused leaching of Fe and Mg and replacement by octahedral Al, leading to formation of dioctahedral clays. Subsequent oxidation of the deposit after uplift and partial erosion has led to minor oxidation and transformation to dioctahedral clays.

For this study, material from the Cretaceous Blue Spur Conglomerate (Craw et al., 1995; Kerr et al., 2017) was selected. Groundwater alteration and cementation of the conglomerate has resulted in formation of diagenetic clays, including abundant green vermiculite (Craw et al., 1995; Kerr et al., 2017). Alteration was almost pervasive through even the largest clasts.

This alteration occurred partly via direct replacement of metamorphic phyllosilicates, and partly via clay re-precipitation as part of the cement. Phengitic muscovite has been illitized with some alteration proceeding to kaolinite. There has been minor oxidation of the deposit after uplift, with associated partial transformation of $Fe^{2+}$ to $Fe^{3+}$ (Craw et al., 1995; Kerr et al., 2017; Malloch et al. 2017).

### 3.2.2. Granby Tuff geological context

The Granby Basaltic Tuff formation is located in the Hartford rift basin of Connecticut and Massachusetts, USA, which is part of the Eastern North American Mesozoic Rift Valley system. The half-graben is filled with terrestrial sediments interspersed with basalt flows. The Granby Tuff itself consists of basalt flows, dikes and sills, well-bedded, grey-to-brown pyroclastic units and tuffaceous sandstones and agglomerates derived from volcanic debris (Robinson and Luttrell, 1985; Schlische, 1993). In places it contains zones of vesicular basalts that have amygdales filled with calcite and dark-brown clays (April and Keller, 1992).

The clays filling the amygdales are of apparent hydrothermal origin, precipitated in gas vesicles from solutions generated by hydrothermal alteration of the basaltic tuff. The clays are well-crystallized, Fe-rich, and trioctahedral 2:1 minerals (April and Keller, 1992). The chemistry of the clay minerals would indicate that they comprise a monomineralic phase, likely saponite, similar as in other purportedly hydrothermal settings. However, the crystallographic data suggests that the clays are rather composed of an intimate mixture of saponite and a low-charge clay mineral resembling vermiculite (April and Keller, 1992). The physical nature of the saponite-vermiculite in Granby Tuffs has not been determined so far.

## 4. Samples and methods

To verify spectral matches of these identified Fe-rich trioctahedral terrestrial vermiculites, we have collected samples from the Otago location and the Granby Tuff. Samples from Otago were collected from the Cretaceous Blue Spur Conglomerate formation, specifically from the location previously studied by Craw et al. (1995). The Blue Spur Conglomerate is a prominent member of the deposits accumulated along faults formed in the Otago region. Collected samples display a range from unoxidized diagenetic alteration to post-depositional oxidation of diagenetically altered rocks and include (1) lithic host rock clasts that represent greenschist facies fragments derived from the basement and scarps, (2) blue-green clay-dominated schists

with abundant vermiculite and (3) paler, oxidized rocks containing Al-phyllosilicates or Fe-oxides, or both (Fig. 3).

To analyze clays in the Granby Tuff basalts, we characterized the same samples that were previously studied by April and Keller (1992). Samples were collected from a Granby Basaltic Tuff exposure in the northern part of Hartford rift basin. The samples contain mm-sized vesicles infilled with clay minerals (Fig. 4) of purportedly hydrothermal origin.

The samples were characterized by X-ray diffraction to understand their chemistry and structure and by NIR spectroscopy in order to provide further structural details and to assess the match to Oxia Planum bedrock clays. For the analysis, 2–3 g aliquots of each bulk sample were crushed and milled to coarse powders (grain size up to 500 μm) in an agate mill for 20 minutes. A fraction of the coarse powder was then further milled with a micromill (McCrone Micronizer Mill) for 10 minutes to prepare the grain size suitable for XRD characterization (grain size below 65 μm).

Bulk rock X-ray diffraction patterns were obtained using a D8 Advance diffractometer (Bruker) equipped with a Cu X-ray tube (wavelength 1.54 Å) and a LynxEye detector. The random powder mounts of the bulk samples were analyzed in a step scan mode from 2° to 65° 2θ with a step increment in 2θ of 0.01° and a count time of 0.3 seconds per step. The mineral phases were identified with a DIFFRAC.EVA search-match module coupled with Crystallography open database and PDF-2.

For more detailed characterization of phyllosilicates, the clay fraction (<2 μm) was separated from the bulk rocks following USGS procedures (Poppe et al., 2001) and analyzed by XRD. 0.5 g of each sample were crushed gently with a mortar and pestle, dissolved in 200 ml of $Na_2CO_3$ for 24 hours to break up flocculated clay particles and agglomerates and the suspension was dispersed by sonification for 10 minutes. The clay fraction was separated from bulk minerals by gravimetric settling (based on flotation and Stoke's law principles) in a beaker for 6 h. After that time, the supernatant was filtered and decanted. To prepare oriented mounts suitable for XRD analysis, the suspension was passed through a 0.45 μm filter and the clay fraction collected was placed on glass slides and allowed to dry.

From prepared oriented mounts, clay minerals were identified by XRD in four analytical steps. First, air-dried samples were scanned with XRD and then solvated with ethylene glycol at 60°C for 24 hours. Such treatment allows for the identification of swelling clays by comparing the d-spacings of air-dried and glycolated samples. Swelling of clays and a shift to larger d-spacing related to swelling was identified by XRD. Next, samples were heated to 350°C

and to 550°C, respectively, to identify clays showing loses of interlayer water leading to a collapse of the structure and a decrease in d-spacing, and clays such as kaolinite that degrade at high temperature. XRD analysis was done in a step scan mode from 2° to 34° 2θ with a step increment in 2θ of 0.01° and a count time of 0.3 seconds per step. The specific clay minerals were identified based on the peak shifts revealed after each treatment.

Near Infrared (NIR) spectra for each sample were collected using a reflectance spectrometer in the near-infrared (0.8–4.2 μm) mode. For this purpose, a Fourier Transform spectrometer (PerkinElmer Spectrum 100N FTNIR) was used. Analysis was performed under ambient temperature and pressure conditions. For the study of powdered samples, the spectral resolution was set to 4 $cm^{-1}$. The collecting spot size of about 1 mm ensured a representative bulk characterization of all components of the powdered material. To calibrate the sample reflectance spectrum, reference spectra were acquired using an Infragold and a Spectralon 99% (Labsphere). An automated correcting mode on the instrument was used to better correct the OH signatures due to ambient air (slightly noisy data are spotted around 1.4, 1.9, and 2.7 μm). Noise present near 2.6 μm does not permit verification of absorption at 2.5 μm such as the one reported to exist locally at Oxia by Mandon et al. (2021).The spectra were processed using a procedure of continuum removal from 1.00 μm to 2.60 μm to compare our laboratory results with CRISM and OMEGA spectra, which are best interpreted by using this part of the signal. For the interpretation, we present the NIR spectral characteristic for each individual sample as well as a linear mixtures of various samples. The linear mixture was obtained by an addition of 20 % of the signal of each sample independently of the wavelength, thus the mixture is qualified as linear.

Both Otago and Granby samples have been added to the newly built analogue rock collection and database of Planetary Terrestrial Analogue Library (PTAL, www.ptal.eu) along with the analytical results performed on the samples and discussed in this paper.

## 5. Results

### 5.1. Otago schists

#### 5.1.1. XRD characterization

The five Otago schist samples reported here contain mostly primary detrital quartz and albite. Some of the samples (e.g., OT-3), contain additional primary metamorphic minerals such as pumpellyite and amphibole (Fig. 5). All five samples contain a variety of phyllosilicates and clay minerals, including micas (muscovite and illite), and expanding clays of the vermiculite,

smectite and chlorite groups. The most pronounced difference among the samples is the presence of amphibole and pumpellyite in sample OT-3, suggesting it is the least altered remnant of the metamorphosed schist. For the remaining samples, differences in the degree of alteration seem to be reflected only in the clay fraction content.

The XRD patterns of oriented clay fraction separates are shown in Fig. 6. The Otago diffractograms differ in terms of the relative heights of peaks, but some general trends of swelling and collapse observed after treatments can be observed, as follows:

- Peaks at 14Å in air-dried samples shift toward 17Å after glycolation and collapse to 10Å after heating to 350°, indicating the presence of an expandable clay mineral. We interpret it as trioctahedral vermiculite, although it is possible that vermiculite is intergrown with smectite.
- A fraction of the 14Å peak is retained after glycolation, but collapses to 12Å after heating to 350° and 550°. This is interpreted to show presence of dioctahedral vermiculite.
- A wide shoulder at 10Å–14Å in air-dried samples shifts towards higher d-spacing values after glycolation and then collapses to 10Å with heat treatment. This feature suggests a mixture of expandable clays with a broad range of d-spacings, which is most likely interstratified illite-vermiculite.
- A peak at 10Å remains broadly unchanged in all treatment stages. We interpret this as illitized muscovite or a similar mica component.
- A peak at 7Å present in air-dried samples remains broadly unchanged after glycolation, but disappears after heating. This is characteristic of either chlorite or kaolinite, or both. In the case of Otago samples, the presence of chlorite is most likely.

Based on the above interpretation, we infer that the least diagenetically altered sample (OT-3) contains chlorite, interstratified illite-vermiculite and minor amounts of trioctahedral vermiculite and mica. The two mesoscopically green samples (OT-1 and OT-2, Fig. 3) contain significant amounts of illitized muscovite (sericite), trioctahedral vermiculite and interstratified illite-vermiculite. Chlorite is present, but is not significant. The mesoscopically whitish, pale samples OT-4 and OT-5 (Fig. 3) differ from the others in terms of vermiculite structure. They contain illitized muscovite, interstratified illite-vermiculite and dioctahedral vermiculite. Trioctahedral vermiculite is absent. A summary of the mineralogy of the samples is given in Table 2 and the XRD patterns are shown in Fig. 6.

### 5.1.2. NIR spectra interpretation

The NIR spectra of Otago samples are shown in Fig. 7 and absorption positions are listed in Table 3 (centers of absorption without continuum removed) and in Table 4 (centers of absorption with continuum removed from 1.00 µm to 2.60 µm). In NIR spectroscopy, all Otago samples show similar absorptions:

- Near 0.96 µm, which can be attributed to electronic transition related to the presence of $Fe^{2+}$ in phyllosilicate;
- Near 1.42; 1.92; 2.78 or 2.83 µm, which can be attributed to presence of OH and $H_2O$ in the phyllosilicate component;
- Near 2.20 µm attributed to Al-OH stretching and bending;
- Near 2.30; 2.34; 2.45 µm, attributed to Fe,Mg-OH, Fe/Mg ratio and oxidation stage of octahedral Fe. The absorption near 2.45 µm is extremely weak and only visible in continuum removed spectra, therefore we do not interpret it further than for Fe/Mg ratio assessment,
- An additional absorption can be distinguished near 2.25–2.26 µm, probably linked to AlFe-OH (King & Clark, 1989).

Based on the features listed above, we interpret that all Otago samples contain substantial amount of $Fe^{2+}$- and $Mg^{2+}$-rich clay minerals with low amounts of $Al^{3+}$, Al + $Fe^{3+}$ and $Fe^{3+}$ rich components in octahedral sites (see table 5 for details). A variety of absorptions distinguishable in the region between 2.00 µm and 2.60 µm can be interpreted towards understanding the diversity of clays present in the mixture. The Fe/Mg ratio is relatively high, although sample OT-3 is visibly more Mg-rich. When the continuum is removed, the absorption near 1.40 µm appears more complex; the absorption near 2.20 µm is shifted towards shorter wavelengths. Also, a distinct absorption is present near 2.30 µm and the absorptions near 2.40-2.50 µm and near 2.70-2.80 µm are shifted towards longer wavelengths. Most of these differences suggest additional components in this clay mixture, whereas the absorptions near 1.40-1.45 µm and 2.70-2.80 µm can be linked to more absorbed $H_2O$ compared to other samples.

To understand the di- versus trioctahedral nature of clays in the Otago samples, the absorptions attributed to the presence of Al are interpreted. The nature of clays in terms of their detailed $Al^{3+}$, Al and $Fe^{3+}$, and $Fe^{2+}$ contents is provided in Table 5. Al-rich clays are present in samples OT-1 and OT-5, but are negligible in the other Otago samples. Instead, samples OT-2, OT-3 and OT-4 contain clays with Al+$Fe^{3+}$ in their structure, while these are absent from OT-1 and OT-5. Due to the complex nature of absorptions, full quantification of the spectra is

impossible. However, in Table 5 we list spectral features and interpret them towards understanding structural types and compositions of clay minerals in Otago samples.

Since laboratory point spectra are not comparable to orbital data in terms of spatial coverage, a linear mixture of all Otago spectra (OT-M) was created. This could mimic a mixture of the different types of samples seen at another scale. The obtained spectrum (OT-M) reveals absorptions suggestive that the dioctahedral component is less important than the trioctahedral (2.20 µm bands are less important than 2.30 µm bands) when compared to other Otago samples. But, both components are still clearly visible and this linear mixture does not change the general interpretations on Otago samples.

The interpretation of the NIR spectra (Fig. 7, Table 3–5) corresponds reasonably well with XRD results (Fig. 6, Table 2) and the general nature of samples. Sample OT-3 contains metamorphic chlorite and is not extensively altered to secondary clay minerals, which agrees well with its spectral characteristic. The presence of Al and Al+$Fe^{3+}$ in the clay structure shown by NIR agrees with the detection of mica-illite and interstratified illite-vermiculite in the samples.

## 5.2. Granby tuffs

### 5.2.1. XRD characterization

Bulk samples of Granby tuff were characterized with XRD. The patterns reveal that all samples contain albite and augite as major rock-forming minerals. Ilmenite and minor amounts of zeolite are present as well (Fig. 8). The samples contain significant amounts of phyllosilicates and clay minerals represented by expanding clays of the vermiculite and smectite group, the chlorite group and possibly a mica-illite component.

The XRD patterns of the oriented clay fraction separates (for two representative samples: GR-2 and GR-5) are presented in Fig. 9. The characteristic peak shifts are observed as listed below:

- A peak at 14Å d-spacing in air-dried samples shifts toward 17Å with glycolation, and collapses to 10Å after heating to 350° and 550°, indicating an expanding clay mineral. We interpret this clay to be a trioctahedral vermiculite. The *001* peaks in diffractograms are associated with *001* reflections at 7Å and 8Å, indicating well the crystallized nature of the clay. The peak at 9.5Å appearing in sample GR-5 after heating to 550°C suggests the clay may be an interstratified mixture of two expandable clay minerals, which

collapse to different d-spacings. We infer that vermiculite is intergrown with saponite, a trioctahedral smectite.

- A weak peak at 10Å (In GR-5 only) remains nearly unchanged in all treatment stages. We interpret this to represent a mica-type mineral, but a full characterization of its mineralogical properties is difficult.

Based on the above interpretation, the clay fraction of the Granby basaltic tuff contains a well crystalline mixture of trioctahedral vermiculite and (likely) saponite. Notably, sample GR-5 contains a larger amount of saponite than sample GR-2. A summary of the mineralogy of these samples is given in table 6 and XRD patterns of the clay fraction are shown in Fig. 9.

### 5.2.2. NIR spectra interpretation

Four samples of Granby tuff were characterized with NIR and the results are shown in Fig. 10. The characteristic absorptions are listed in table 7 (centers of absorption without continuum removed) and table 8 (centers of absorption with continuum removed from 1.00 µm to 2.60 µm). In NIR spectroscopy, all Granby samples show similar absorptions:

- Near 1.41; 1.91; 2.76 µm, which are linked to OH and $H_2O$ in phyllosilicate component;
- Near 2.20 µm, attributed to Al-OH stretching and bending;
- Near 2.21; 2.31; 2.35; 2.40 µm which are characteristic for Fe,Mg-OH vibrations (King & Clark, 1989).
- An extremely weak absorption near 2.40 µm, which is only clearly visible when the continuum is removed (Fig. 10b, Table 8). Therefore, it cannot be interpreted with large confidence towards the assessment of the Fe/Mg ratio.
- An absorption at 2.43 µm is seen in sample GR-5 but not in GR-2.

The samples show spectral differences mainly in the absorptions patterns between 2.25 and 2.50 µm. The absorption near 2.30 µm is closer to 2.30 µm in GR-1 and GR-5, while for GR-2 and GR-3 it is closer to 2.32 µm. GR-2 shows an absorption near 2.35 µm, hidden in the shoulder of the stronger absorption around 2.30 µm, which is stronger than for any other sample. These shifts of absorption peaks relate probably to different Fe/Mg ratios (King & Clark, 1989), and would mean that sample GR-2 is richest in $Fe^{2+}$. Absorptions near 2.30 µm and 2.35 µm in continuum removed spectra, are combined in one bigger absorption and its position and strength should not be used in estimating the Fe/Mg ratio.

If analysed with the continuum removed, GR-2 is the only sample to have a clear feature near 2.50 µm, while having a weaker and narrower absorption near 2.40 µm. The latter

absorption is also weak and thin in the GR-3 sample compared to GR-1 and GR-5 samples. Interestingly, this is inversely correlated to the strength of the absorption near 2.30 µm that is stronger in GR-2 and GR-3 compared to GR-1 and GR-5. To interpret the iron content and speciation, the absorption near 1.00 µm linked to $Fe^{2+}$ is stronger in GR-2 and GR-3 compared to GR-1 and GR-5. This could imply a different Fe/Mg ratio for GR-1 and GR-5 than in GR-2 and GR-3. GR-2 and GR-3 samples have probably more $Fe^{2+}$ than GR-1 and GR-5.

NIR spectra of all four Granby samples suggest the presence of a nearly pure trioctahedral clay mineral, rich in $Fe^{2+}$ and $Mg^{2+}$, and with low amounts of $Al^{3+}$ (Table 9). The main distinction observed for the Granby samples relates to a slight difference in the Fe/Mg ratio.

## 6. Discussion

The samples collected from both the Otago and Granby locations contain Fe-rich trioctahedral clay minerals, which - with some certainty - we confirm to be vermiculite or a mixture of vermiculite and Fe-saponite. Our goal was to find natural terrestrial samples that provide a spectral match between these rocks and Oxia Planum bedrock deposit phyllosilicates to better understand the mineralogy of this site. The geological context of vermiculite formation in analogue sites allows us to address, to some extent what possible processes, such as aqueous alteration, involved in formation of the bedrock deposits at Oxia Planum. Below we discuss these as well as questions related to organic matter and the preservation potential of biosignatures.

### 6.1. Otago and Granby vermiculite – Spectral comparison with Oxia bedrock deposits

In NIR spectra, Otago vermiculite-bearing rocks reveal absorptions near 1.00 µm; 1.40 µm; 1.90 µm (absorptions 1, 2, 3), which are all similar to absorptions present in spectra from Oxia Planum (Table 1 versus Table 2; Fig. 11). This means that the nature and overall Fe content of the phyllosilicates at Oxia are likely to be broadly similar to the clays from Otago sediments.

The Otago samples reveal strong absorption near 2.20 µm, which is attributed to the presence of an Al-bearing clay component such as illite or interstratified vermiculite-illite. Absorption varies from one sample to another, increasing with more advanced illitization of vermiculite. For Oxia Planum, this absorption is seen with OMEGA only, and not with CRISM, i.e., only at low spatial resolution. Spectral comparison of Otago clays to Oxia in this respect suggests that Al content and $Al+Fe^{3+}$ substitution is minor or absent at Oxia, but any 2.20 µm band in Oxia spectra would be attributed to presence of illite that forms from vermiculite alteration.

Some spectral differences occur in the absorptions near 2.30 µm and near 2.40 µm. Especially the absorption near 2.30 µm that is at a longer wavelength (2.34 µm for Otago), meaning most likely that the Otago vermiculite ratios of $Fe^{2+}/(Fe^{3+}+Fe^{2+})$ and $Fe^{2+}/(Mg+Fe^{2+})$ are higher than those for Oxia's minerals. It is known that for Otago vermiculite, the ratios are 0.7 and 0.6, respectively (Craw, 1984). This is consistent with the absorption near 2.40 µm, that is at longer wavelengths in Otago samples.

In the case of the Granby Tuff samples, the relative strength of the absorptions near 1.00, 1.40, 1.90, 2.20 and 2.30 µm and their positions are similar to those of Oxia Planum (see Table 1 versus Table 7; Fig. 11). In addition, spectral variations from sample to sample are very similar to those seen over the Oxia region, making the Granby samples a very good analogue to Oxia Planum bedrock deposits. However, all Granby samples reveal a weak absorption near 2.35 µm (Table 7, also Fig. 10c) that is lacking in Oxia Planum spectra. Additionally, the 2.39 µm absorption typical for Oxia Planum is very weak in Granby samples and only visible in the spectra with continuum removed. This suggests that the Granby clays have different Fe/Mg ratios than minerals of Oxia Planum, or a different (plausibly lower) oxidation state for Fe in the clay structure. An absorption near 2.35 µm present in Granby but not in Oxia spectra is diagnostic of the presence of $Fe^{2+}$-saponite (Neuman et al, 2011). Indeed, Granby samples contain a vermiculite-saponite mixture (Fig. 9). Lack of spectral analogy of Granby samples to Oxia rock exposures in this aspect indicate Oxia Planum phyllosilicates to be rather a pure vermiculite than a saponite-bearing mixture (Fig. 11). This is consistent with large homogeneity of spectral signatures of Oxia bedrock phyllosilicates and suggests a relatively homogeneous composition of these deposits.

Both Granby and Otago samples present a more complex combination of absorptions near 2.20, 2.30 and 2.35 µm than at Oxia and present a weaker absorption near 2.39 µm. This can be interpreted as a more complex mixture of clays in the Granby and Otago samples leading to a set of absorptions linked to various vibrations of Al-OH, AlFe-OH, Fe-OH and Mg-OH compared to Oxia. The latter displays its main absorption near 2.32 µm (sometimes associated with a weak feature near 2.20 µm) and a weaker feature near 2.39 µm. Overall, Oxia Planum clays most likely contain a less complex clay mineral assemblage than those comprising the Granby and Otago examples (Fig. 11). However, comparing laboratory and remote sensing data, limitations must be considered. Such differences in complexity can be apparent, resulting from the different scale of observation, i.e. point data collected in the laboratory compared to remotely-sensed spectra acquired from meter-large areas. However, it is likely that no significant spectral artefacts are created, such as missing bands or the presence of extra bands,

despite differences in the scale of observation. The spectral resolutions of our laboratory samples and remote-sensing data are comparable, therefore the effect of scale of observation can be excluded. Specific matrix effect of sample is the only possibility that would affect the complexity of the spectra, but this remains a hypothesis to be tested in the future.

### 6.2. Imperfect spectral matches - Implications for understanding the geological environment at Oxia Planum

Our study shows that rocks containing Fe-rich trioctahedral vermiculite, with limited amounts of octahedral Al and $Fe^{3+}$ (subject to the validity of any absorption near 2.20 μm) are likely the main component of bedrock phyllosilicates at Oxia Planum. If this is the case, understanding the pathways of vermiculite formation in the terrestrial sites, may shed new light on the aqueous evolution at Oxia Planum. The terrestrial sites that we analysed represent (1) vermiculitized chlorite-schists, which underwent alteration processes without significant oxidation (Otago) and (2) basaltic tuffs with Fe-rich clays filling amygdales of supposedly hydrothermal origin (Granby). As stated in the section 3.1, vermiculite forms by aqueous alteration of either chlorite or mica and in order to retain the trioctahedral nature of the mineral, anoxic conditions must be present during alteration (Fig. 2). Our results cannot be used to argue for the origin of the primary mineral, and for instance low-grade metamorphic origin of primary chlorite in Otago does not have to imply that such a process played a role in the setting of the layered clays at Oxia Planum. However, the results point to some critical conditions (such as lack of oxidation during alteration) that must have been valid during aqueous alteration and therefore can be used to understand aqueous processes at Oxia Planum.

Based on geomorphological evidence, bedrock clay deposits at Oxia Planum could have formed either in a subaqueous environment (palustrine, lacustrine or marine), or in subaerial conditions compatible with airborne volcaniclastics altered by pedogenesis or aeolian deposits (Carter et al., 2016; Turner and Bridges, 2017; Quantin-Nataf et al., 2020, Mandon et al. 2021). Deep burial and metamorphic conditions do not seem likely (Quantin-Nataf et al. 2020). Additionally, the fact that the bedrock unit drapes the paleo-topography at a regional scale (Quantin-Nataf et al., 2020), favours either a sedimentary origin of the deposits, or air-fall deposition (e.g. ash-fall). Below we discuss constraints arising from our results considering known geological context of the Oxia bedrock formation.

The clay minerals present in the Granby Tuff provide a good spectral analogue to the clays of Oxia Planum in that they have similar 2:1 structure, are mainly trioctahedral and appear to contain little Al in tetrahedral positions. The Granby phyllosilicates likely formed by

precipitation from hydrothermal-related processes, such as suggested on Mars byMeunier et al. (2012). . Oxia bedrock clays differ from Granby Tuffs in their Fe/Mg ratio and Fe oxidation state. This may mean that Oxia clays had undergone post-formation oxidation or alteration in a water-rich environment. As shown for Martian smectites, the prevailing occurrences of Fe-rich clays over Mg-rich clays is due to various degrees of leaching of Mg and Fe from primary material and subsequent segregation of Fe and Mg (Michalski et al., 2015). Taking into account the ability of Fe to oxidize when transported in water-rich conditions, the primary oxidation state of Fe in vermiculite could be changed slightly by post-formation processes affecting clays (Murakami et al., 2004).

Alternatively, if phyllosilicates at Oxia Planum are derived from ash-fall deposits, their high Fe content may be a consequence of the primary enrichment of Fe in the martian mantle (Morgan and Anders, 1979; Taylor, 2013) resulting in greater amounts of Fe in Martian volcanic source magmas compared to their terrestrial counterparts (e.g., Boynton et al., 2009; Papike et al., 2009; Treiman et al., 2014) as

Spectral analogies and lack thereof for vermiculite in the altered Otago schists and bedrock deposits at Oxia Planum shed some light on the conditions during possibly sedimentary processes to form bedrock at Oxia. First, vermiculite is inconsistent with authigenic precipitation and sedimentation, as it is an alteration product of chlorite or mica (see Fig. 2). In such a context, the presence of vermiculite implies transport of the mineral from elsewhere. Second, the trioctahedral nature of vermiculite is consistent with anoxic conditions during aqueous alteration. Third, at the Otago geological site, only after exhumation of vermiculite, progressive oxidation and illitization took place leading to a change of Al + $Fe^{3+}$ clay characteristics (Craw et al., 1995). Oxia Planum bedrock deposits lack any spectral feature that in Otago samples results from illitization. Therefore, lack of Al in Oxia clays implies that, if clays are of sedimentary origin, subsequent alteration must have occurred in non-oxidizing conditions, at a low water to rock ratio and the deposits were not oxidized nor altered after deposition, so that illitization did not progress.

In summary, our results suggest that Oxia Planum bedrock clay deposits are composed of an Fe-rich, trioctahedral vermiculite-like mineral. This type of material could have been formed by processes associated with hydrothermal alteration operating during the Noachian time and later been deposited at Oxia.

If deposits at Oxia Planum were laid down by sedimentary processes, then the clays may have formed elsewhere and were later transported and deposited under anoxic, aqueous

conditions. In both cases, deposits must have been slightly buried and protected from pedogenic alteration, which otherwise would cause oxidation and illitization.

### 6.3. Implications for the preservation of organic matter and biosignatures

The overarching goal of the ExoMars 2022 rover mission is to search for biosignatures of Martian ancient life forms and to perform analysis on organic matter plausibly preserved in the Martian subsurface (Vago et al., 2017). Clays are important minerals from the point of view of organic matter preservation. Storage of organic matter in these minerals is related to their cation exchange capacity (CEC), i.e. the quantity of readily exchangeable cations neutralizing negative charges. CEC is controlled by cation and anion substitutions in the tetrahedral or octahedral sheet, which create charge deficits that enable adsorption of organic molecules at particle edges. Trioctahedral vermiculite has a CEC in the range of 130–200 meq/100 g (Ghabru et al., 1989) and this is significantly higher than the capacity of smectites, which ranges between 70 and 130 meq/100g (Weaver and Pollard, 1973). Therefore, has a high potential to adsorb and store organic matter. Thecapacity of clay minerals to store organic matter is highly related to their Fe content and oxidation state. As shown analytically and experimentally on natural soils, leaching of Fe from clay structure and formation of Fe-oxides significantly decreased organic matter retention capacity (Wiseman and Püttmann, 2006; Sodano et al., 2016). As such, trioctahedral, Fe-rich vermiculite thought to form vast deposits at Oxia Planum has a great potential to store organic matter.

In order to preserve organic matter for long periods of geological time, however, adequate geological and geochemical conditions must operate. Geological context of vermiculite deposits at Oxia Planum (Quantin-Nataf et al., 2020), namely indications of material being transported from a large catchment area and depositedand buried in a large basin, makes preservation of organic material promising.

Only two analogue sites were studied here. However, our results shed some light on geochemical and environmental conditions operating at Oxia Planum during and after deposition of bedrock phyllosilicates. If vermiculite formed in association with hydrothermal processes elsewhere and was later deposited at Oxia Planum as we postulate above, the preservation of organic matter depends on the hydrothermal conditions (e.g., Summons et al., 2011) and our data do not allow for extended discussion. Results suggest little to no oxidation of vermiculite after sediment deposition at Oxia. The absence of oxidizing conditions in sedimentary environments increases the chances for the preservation of organic matter.

Our second analogue site studies suggest that vermiculite could have formed by alteration under reducing, anoxic conditions. In such a case, the concentration and preservation of any

organic matter would likely be enhanced. It is important to note that in the case of the Otago schist, the presence of organic matter within the deposits was indeed an important factor to inhibit oxidation of vermiculite (Tostevin et al., 2017). Additionally, lack of signatures of post-depositional oxidation (and illitization) of vermiculite at Oxia increases chances of organic matter preservation in the deposits.

## 7. Conclusions

We have performed a survey of vermiculite-bearing terrestrial rocks to identify mineralogical and spectroscopic analogues for bedrock clay deposits present at the Oxia Planum, the ESA-Roscosmos ExoMars2022 landing site. Based on the analysis of NIR spectra of Oxia Planum bedrock phyllosilicate deposits and previous interpretations, we focused on locating specimens of Fe-rich trioctahedral vermiculite from occurrences identified in the literature. Two terrestrial sites that fulfil the spectral match requirement were identified. These sites are (1) vermiculitized chlorite-schists from Otago, New Zealand, which underwent an alteration process without significant oxidation and (2) basaltic tuffs from Granby, Massachusetts, USA, with Fe-rich clays filling amygdales of supposedly hydrothermal origin.

The spectral comparisons of these analogue rocks and Oxia bedrock confirms that Fe-rich trioctahedral vermiculite is the most likely phyllosilicate that comprises Oxia's deposits. In terms of clay structure and its di- versus trioctahedral nature, Oxia bedrock clay-rich deposits are matched best by vermiculite-saponite mixtures in basaltic rock amygdales occurring in the Granby Tuff, although contribution of saponite must be minor at Oxia Planum. Phyllosilicates at Oxia Planum are rich in Fe and contain more oxidized $Fe^{3+}$ than the Granby clays. These differences may be explained by the higher iron content of Martian minerals overall, and by the post-depositional oxidation of Oxia Planum phyllosilicates in an aqueous environment.

Otago vermiculite could be a good analogue to Oxia vermiculite in terms of overall mineralogy and Fe content, but several spectral inconsistencies reveal that alteration of chlorite, if this led to formation of bedrock deposits at the Oxia, occurred with limited oxidation. Illitization of vermiculite, which results from post-alteration oxidation in Otago, is not observed for Oxia clays. Additionally, preserving $Fe^{2+}$ in the vermiculite structure implies limited water-rock interactions in reducing conditions during deposition of bedrock minerals.

The spectral match between vermiculite from terrestrial environments and bedrock deposits at Oxia Planum provides strong evidence sn for the mineralogy of Oxia bedrock. If the clays are in fact mainly vermiculite, then our results along with geomorphological observations suggest that the deposits at Oxia Planum may have been deposited as ash-fall deposits or in a

sedimentary setting by transport and aqueous alteration of primary minerals from elsewhere. Neither authigenic precipitation or in situ advanced pedogenic alteration of sediments are likely processes for the formation of vermiculite.

**Acknowledgments:** This project has received funding from the European Union's Horizon 2020 (H2020-COMPET-2015) Research and Innovation Program under grant agreement 687302 (PTAL), as well as the Research Council of Norway through its Centres of Excellence funding scheme, project number 223272. We thank Ibrahim Khaled and Thanusha Naidoo for their kind assistance in XRD sample preparation and data collection and Paul Schofield for help in bulk rock XRD patterns interpretation. Two anonymous reviewers are greatly acknowledged for their comments on the first version of the manuscript and Lucia Mandon for sharing with us the unpublished version of her manuscript.

**Supplementary material**: XRD patterns and NIR spectra of all samples are freely available as part of the PTAL database (currently http://erica.uva.es/PTAL/).

## References

1. April R.H. and Keller D.M., 1992: Saponite and vermiculite in amygdales of the Granby basaltic tuff, Connecticut Valley. Clays and Clay Minerals 40: 22-31.
2. Badaut D., Besson G., Decarreau A., Rautureau R. 1985: Occurrence of a ferrous, trioctahedral smectite in recent sediments of Atlantis II Deep red Sea. Clay Minerals 20: 389-404.
3. Basset W.A., 1959. The geology of vermiculite occurrences. 10th National Conference on Clays and Clay Minerals: 61-69.
4. Bibring, J-P., et al. "OMEGA: Observatoire pour la Minéralogie, l'Eau, les Glaces et l'Activité." Mars Express: the scientific payload. Vol. 1240. 2004.
5. Bishop D.G., 1972: Progressive Metamorphism from Prehnite-Pumpellyite to Greenschist Facies in the Dansey Pass Area, Otago, New Zealand. Geological Society of America Bulletin 83: 3177-3198.
6. Bishop D.G. and Turnbull I.M., 1996: Geology of Dunedin area. GNS Science 1:250 000 Geological Map, Lower Hutt, New Zealand. Sheet 21. 52pp.

7. Boynton W.V., Taylor G.J., Karunatillake S., Reedy R.C., Kellet M., 2998: Elemental abundances determined via the Mars Odyssey GRS. In: Bell J. (ed.) The Martian Surface, pp. 105-124.
8. Brown E.H., 1967: The greenschist facies in part of eastern Otago, New Zealand. Contrib. Mineral. Petrol. 14: 259-292.
9. Bultel, B. et al. Description of CoTCAT (Complement to CRISM Analysis Toolkit). EEE Journal of Selected Topics in Applied Earth Observations and Remote Sensing 8 (6), 3039-3049.
10. Campos A., Moreno S., Molina R., 2009: Characterization of vermiculite by XRD and spectroscopic techniques. Earth Sci. Res. Journal 13: 108-118.
11. Carter J., Quantin C., Thollot P., Loizeau D., Ody A., Lozach L., 2016: Oxia Planum, a clay-laden landing site proposed for the ExoMars rover mission: aqueous mineralogy and alteration scenarios. 47$^{th}$ Lunar and Planetary Science Conference. Abstract no. 2064.,
12. Clark, R. N., King, T. V., Klejwa, M., Swayze, G. A., & Vergo, N. (1990). High spectral resolution reflectance spectroscopy of minerals. Journal of Geophysical Research: Solid Earth, 95(B8), 12653-12680.
13. Craw D., 1984: Ferrous-iron-bearing vermiculite-smectite series formed during alteration of chlorite to kaolinite, Otago Schist, New Zealand. Clay Minerals 19: 509-520.
14. Craw D., Smith D.W., Youngson J.H. 1995: Formation of authigenic $Fe^{2+}$-bearing Craw D., 2010: Dealyed accumulation of placers during exhumation of orogenic gold in southern New Zealand. Ore Geology Reviews 37: 224-235.
15. Craw D., Smith D.W., Youngson J.H. 1995: Formation of authigenic Fe2+-bearing smectite-vermiculite during terrestrial diagenesis, southern New Zealand. New Zealand Journal of Geology and geophysics 38: 151-158.
16. Ehlmann B.L., Mustard J.F., Clark R.N., Swayze G.A., Murchie S.L., 2011: Evidence for low-grade metamorphism, hydrothermal alteration, and diagenesis on mars from phyllosilicate mineral assemblages. Clays and Clay Minerals 59: 359-377.
17. Els B.G., Youngson J.H., Craw D., 2002: Blue Spur Conglomerate: Auriferous Late Cretaceous fluvial channel deposits adjacent to normal fault scarps, southeast Otago, New Zealand. New Zealand Journal of geology and Geophysics 46: 123-139.

734 18. Fanning D.S., Keramida V.Z., El-Desoky M.A., 1989: Micas. In: J.B. Dixon and S.B:,
735 Weed (eds.) Minerals in Soil Environments. Soil Science Society of America,
736 Madison, Wisconsin. Pp 551-634.
737 19. Farmer J.D., and Des Marais D.J, 1999: Exploring for a record of ancient Martian life.
738 Journal of Geophysical research 104: E11, 26977-26995.
739 20. Ghabru S.K., Mermut A.R., Arnaud J.R.St., 1989: Layer-Charge and Cation-Exchange
740 Characteristics of Vermiculite (Weathered Biotite) Isolated from a Gray Luvisol in
741 Northeastern Saskatchewan. Clays and Clay Minerals 37: 164-172.
742 21. Gilkes R.J., Young R.C., Quirk J.P., 1972: The oxidation of octahedral iron in biotite.
743 Clays and Clay Minerals 20:303-315.
744 22. Hunt, G. R. (1970). Visible and near-infrared spectra of minerals and rocks: I silicate
745 minerals. *Modern Geology*, *1*, 283-300.
746 23. Hunt, G. R. (1977). Spectral signatures of particulate minerals in the visible and near
747 infrared. Geophysics, 42(3), 501-513.
748 24. Kerr G., Malloch K., Lilly K., Craw D., 2017: Diagenetic alteration of a Mesozoic
749 fluvial gold placer deposit, southern New Zealand. Ore Geology Reviews 83: 14-29.
750 25. King, T. V., & Clark, R. N. (1989). Spectral characteristics of chlorites and Mg-
751 serpentines using high-resolution reflectance spectroscopy. Journal of Geophysical
752 Research: Solid Earth, 94(B10), 13997-14008.
753 26. Kodama H., DeKimpe C.R., Dejou J., 1988: Ferrian saponite in a gabbro saprolite at
754 Mont Meganic, Quebec. Clays and Clay Minerals 36: 102-110.
755 27. Krasnova N.I., Balaganskaya E.G., Garcia D., 2004: Kovdor – classic phoscorites and
756 carbonatites.In: Phoscorites nad Carbonatites from Mantle to Mine: the Key Example
757 of the Kola Alkaline Province (eds: Zaitsev A., Wall F.) Mineralogical Society Series
758 10 pp 95-127. Mineralogical Society London.
759 28. Lantz C., Poulet F., Loizeau D., Rui L., Pilorget C., Carter J., Dypvik H., Rull F.,
760 Werner S.C., 2020: Planetary terrestrial Analogue Library project: 1. Characterization
761 of samples by near-infrared point spectrometer. Planetary and Space Science 189:
762 104989.
763 29. Makumbi L., Herbillon A., 1972: Vermiculitisation expérimentale d'une chlorite.
764 Bulletin du Groupe français des argiles 24: 153-164.
765 30. Malloch K., Kerr G., Craw D., 2017: Placer gold in the Cretaceous Blue Spur
766 Conglomerate at Waitahuna, southern New Zealand. New Zealand Journal of Geology
767 and Geophysics 60: 239-254.

31. Mandon, L., et al. 2021: Morphological and spectral diversity of the clay-bearing unit at the ExoMars landing site Oxia Planum. Astrobiology, accepted.
32. Meunier A., Petit S., Ehlmann B.L., Dudoignon P., Westall F., Mas A., El Albani A., Ferrage E., 2012: Magmatic precipitation as a possible origin of Noachian clay minerlas on Amrs. Nature geoscience 5: 739-743.
33. Michalski J.R., Cuadros J., Bishop J.L., Dyar D., Dekov V., Fiore S., 2015. Constraints on the crystal-chemistry of Fe/Mg-rich smectitic clays on Mars and link to global alteration trends. Earth and Planetary Science Letters 427: 215-225.
34. Morgan J.W., and Anders E., 1979: Chemical composition of Mars. Geochimica et Cosmochimica Acta 43: 1601–1610.
35. Mortensen J.K., Craw D., MacKenzie D.J., Gabites J.E., Ullrich T. 2010: Age and origin of orogenic gold mineralisation in the Otago schist belt, South Island, New Zealand: Constraints from lead isotope and $^{40}Ar/^{39}Ar$ dating studies. Economic Geology 105:777-793.
36. Murakami T., Isobe H., Sato T., Ohnuki T., 1996: Weathering of chlorite in a quartz-chlorite schist: I. Mineralogical and chemical changes. Clays and Clay Minerals 44: 244-256.
37. Murakami T., Ito J.-I., Utsunomiya S., Kasama T., Kozai N., Ohnuki T. 2004: Anoxic dissolution processes of biotite: Implications for Fe behavior during Archean weathering. Earth and Planetary Science Letters 224: 117-129.
38. Mustard, J. F. (1992). Chemical analysis of actinolite from reflectance spectra. *American Mineralogist*, *77*(3-4), 345-358.
39. Newman A.C.D. and Brown G., 1987: The chemical constitution of clays. In: Chemistry of Clays and Clay Minerals. Ed: A.C.D. Newman. Mineral. Soc. Monograph 6. Willey-Interscience, 480pp.
40. Neumann, A., Petit, S., & Hofstetter, T. B. 2011 : Evaluation of redox-active iron sites in smectites using middle and near infrared spectroscopy. Geochimica et Cosmochimica Acta, 75(9), 2336-2355.
41. Papike J.J., Karner J.M., Shearer C.K., Burger P.V., 2009: Silicate mineralogy of martian meteorites. Geochmica et Cosmochimica Acta 73: 7443-7485.
42. Poppe L.J., Paskevich V.F., Hathaway J.C., Blackwood D.S., 2001: A laboratory manual for X-ray powder diffraction. US Geological Survey Publication Open-file Report 2001-41.

801 43. Proust D., Eymery J.-P., Beaufort D., 1986: Supergene Vermiculitization of a
802 Magnesian Chlorite: Iron and Magnesium Removal Processes. Clays and Clay
803 Minerals 34: 572-580.
804 44. Robinson P. and Luttrell G.W 1985: Revision of some stratigraphic names in central
805 Massachusetts. In: Stratigraphic Notes US Geological Survey Bulletin 1605-A: A71-
806 A78.
807 45. Ruiz Cruz M.D., 1999: New data for metamorphic vermiculite. European Journal of
808 Mineralogy 11: 533-548.
809 46. Ross G.J., Kodama H., 1976: Experimental alteration of a chlorite into a regularly
810 interstratified chlorite-vermiculite by chemical oxidation. Clays and Clay Minerals 24:
811 183-190.
812 47. Schlische R.W., 1993: Anatomy and evolution of the Triassic-Jurassic continental rift
813 system, Eastern North America. Tectonics 12: 1026-1042.
814 48. Schoeman J.J., 1989: Mica and vermiculite in South Africa. Journal of South Africa
815 Inst. Min. Metall 89: 1-12.
816 49. Semprich J., Schwenzer S.P., Treiman A.H., Filiberto J., 2019: Phase Equilibria
817 Modelling of Low-Grade Metamorphic Martian Rocks. Journal of Geophysical
818 Research Planet 124: 681-702.
819 50. Sodano, M., Said-Pullicino, D., Fiori, A. F., Catoni, M., Martin, M., Celi, L., 2016:
820 Sorption of paddy soil-derived dissolved organic matter on hydrous iron oxide–
821 vermiculite mineral phases. Geoderma 261: 169-177.
822 51. Sugimori H., Yokoyama T., Murakami T., 2009. Kinetics of biotite dissolution and Fe
823 behavior under low $O_2$ conditions and their implications for Precambrian weathering.
824 Geochimica et Cosmochimica Acta 73: 3767-3781.
825 52. Summons, Roger E., et al. "Preservation of martian organic and environmental
826 records: final report of the Mars Biosignature Working Group." *Astrobiology* 11.2
827 (2011): 157-181.
828 53. Taylor G.J., 2013: The bulk composition of Mars. Chemie der Erde, Geochemistry 73:
829 401–420.
830 54. Tostevin R, Craw D, van Hale R, Vaughan M 2016. Sources of environmental sulfur
831 in the groundwater system, southern New Zealand. *Applied Geochemistry* 70: 1-16.
832 55. Treiman A.H., Morris R.V., Agresti D.G., Graff T.G., Achilles C.N., Rampe E.B.,
833 Bristow T.F., Ming D.W., Blake D.F., Vaniman D.T., Bish D.L., Chipera S.J.,
834 Morrison S.M., Downs R.T., 2014. Perrian saponite from the Santa Monica Mountains

(California, USA, Earth): Characterization as an analog for clay minerals on Mars with application to Yellowknife Bay in Gale Crater. American Mineralogist 99: 2234-2250.

56. Turner S.M.R. and Bridges J.C. 2017: Mineralogical analysis of ExoMars rover landing sites using CRISM. 48th Lunar and Planetary Science Conference. Abstract no. 2228.
57. Quantin C. Carter J., Thollot P., Broyer J., Lozach L., Davis J., Grindrod P., Pajola M., Baratti EE., Rossato S., Allemand P., Bultel B., Leyrat C., Fernando J., Ody A., 2016: Oxia Planum, the landing site for ExoMars2018. 47th Lunar and Planetary Sceince Coneference. Abstract no. 2863.
58. Quantin-Nataf C., Carter J., Mandon L., Thollot P., Balme M., Volat M., Pan L., Loizeau D., Millot C., BretonS., Dehouck E., Fawdon P., Gupta S., Davis J., Brindrod P.M., Pacifici A., Bultel B., Allemand P., Ody A., Lozach L., Broyer J., 2020: Oxia Planum – the landing site for the ExoMars 'Rosalind Franklin' Rover Mission: geological context and pre-landing interpretation. Astrobiology.
59. Vago J.L., Westall F., Pasteur Instrument Teams, Landing Site Selection Working Group, and Other Contributors, Coates A.J., Jaumann R., Korablev O., Ciarletti V., Mitrofanov I., Josset J.-L., De Sanctis M.C., Bibring J.-P., Rull F., Goesmann F., Steininger H., Goetz W., Brinckerhoff W., Szopa C., Raulin F., Westall F., Edwards H.G. M., Whyte L. G., Fairén A.G., Bibring J.-P., Bridges J., Hauber E., Ori G. G., Werner S., Loizeau D., Kuzmin R.O., Williams R.M. E., Flahaut J., Forget F., Vago J. L., Rodionov D., Korablev O., SvedhemH., Sefton-Nash E., Kminek G., Lorenzoni L., Joudrier L., Mikhailov V., Zashchirinskiy A., Alexashkin S., Calantropio F., Merlo A., Poulakis P., Witasse O., Bayle O., Bayón S., Meierhenrich U., Carter J., García-Ruiz J.M., Baglioni P., Haldemann A., Ball A.J., Debus A, Lindner R., Haessig F., Monteiro D., Trautner R., Voland C., Rebeyre P., Goulty D., Didot F., Durrant S., Zekri E., Koschny D., Toni A., Visentin G, Zwick M., van Winnendael M., Azkarate M., Carreau C., and the ExoMars Project Team., 2017: Habitability on Early Mars and the Search for Biosignatures with the ExoMars Rover. Astrobiology 17:6-7, 471-510.
60. Vago, J.L., et al. 2017: Habitability on early Mars and the search for biosignatures with the ExoMars Rover. Astrobiology 17: 471-510.
61. Vam Gosen B.S., Bush A.L., 2001: Colarado vermiculite deposits: Mines, Prospects, and Occurrences. US Geological Survey Open-File Repost. OF-01-475.

62. Velde B. and Meunier A., 2008: The Origin of Clay Minerals in Soils and Weathered Rocks. 406 pp. Springer-Verlag.
63. Veneranda M., Manrique-Martinez J.A., Lopez-Reyes G., Medina J., Torre-Fdez I., Castro K., Madariaga J.M., Lantz C., Poulet F., Krzesińska A.M., Hellevang H., Werner S.C., Rull F., 2019: Spectroscopic study of olivine-bearing rocks and its relevance to the ExoMars rover mission. Spectrochimica Acta Part A: Molecular and Biomolecular Spectroscopy: 223: 117360.
64. Weaver C.E., and Pollard L.D., 1973 : The Chemistry of Clay Minerals Developments in Sedimentology. Vol 15 : 213pp. Elsevier Scientific Publishing Company, Amsterdam, London, New York.
65. Wey P.R., Le Dred R., 1972: Vermicuite et vermiculitisation. Bulletin du Groupe français des argiles 24: 111-134.
66. Wiseman, C. L. S., and Püttmann, W., 2006 : Interactions between mineral phases in the preservation of soil organic matter. Geoderma, 134 : 109-118.

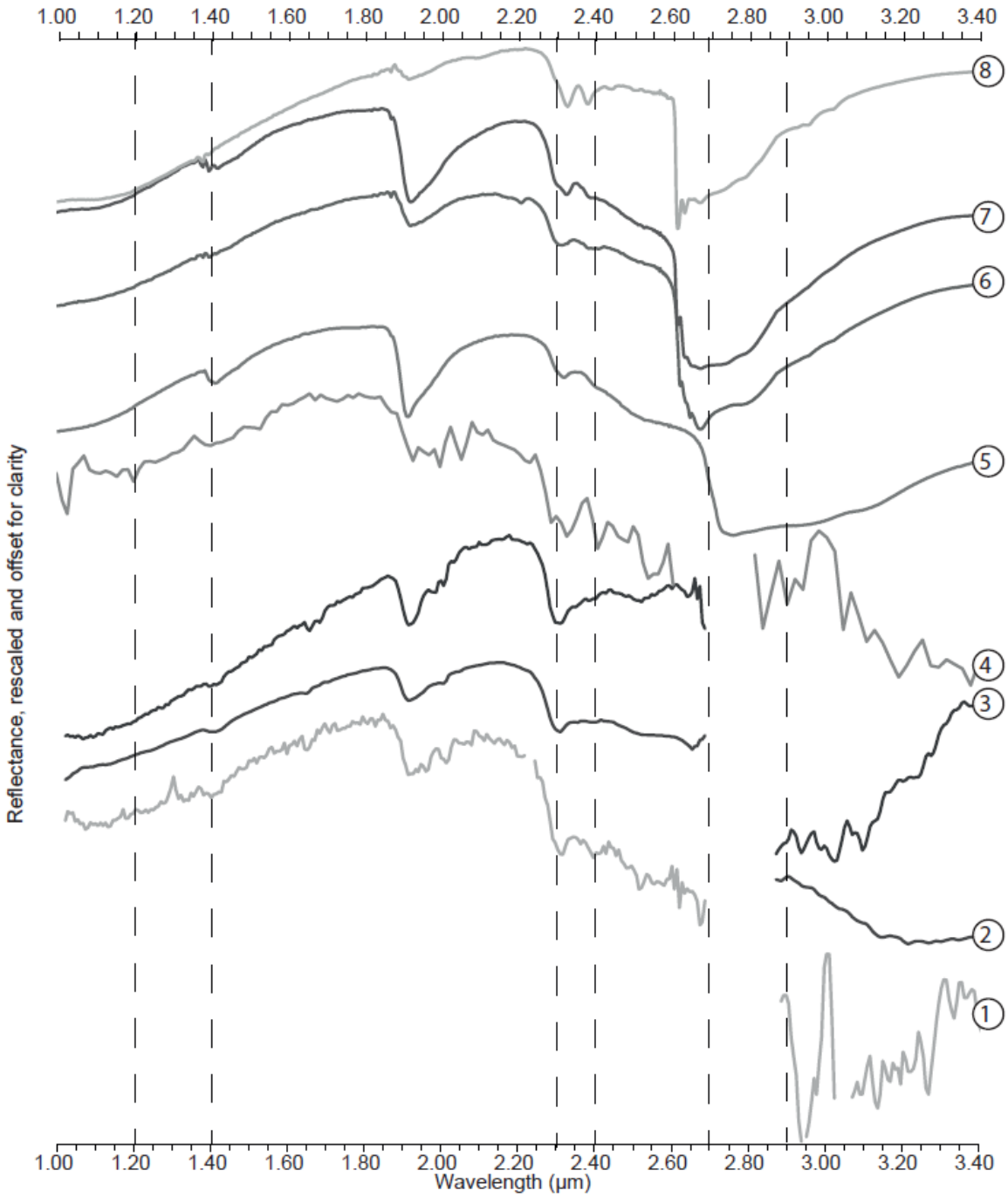


Fig 1. NIR spectrum of Oxia Planum and characteristic spectral features marked: a weak V-shaped absorption near 1.40 µm a large and deep V-shaped absorption near 1.92 µm, a deep absorption near 2.31–2.32 µm, and a weak absorption near 2.38–2.41 µm. Finally, a large and deep absorption is present near 2.90–2.95 µm (for interpretation of specific absorptions, see table 1).

Spectrum 1 is from ATU380B9, it is the median spectrum of an ROI and was drawn by hand on pixels highlighted by spectral criterion “Fe-Mg-vermiculite” of MarsSI (Quantin et al, 2018) data to minimize the noise and maximize the signal (110 pixels: around x: 314; y: 89, non-projected). Spectrum 2 is from FRT810D, the spectral criterion from Bultel et al, 2019 (BDa23) is applied on the cube and an automatic Region of Interest (ROI) for all pixel with an absorption >5% (18483 pixels) is determined. Spectrum 3 is from FRT810D, an ROI drawn by hand on the pixels highlighted by the spectral criterion from Bultel et al, 2019 (BDa23) on

a restricted area on the centre of the CRISM image (352 pixels: around: x:302; y: 192, non-projected). Spectrum 4 is from an ROI ORB5307_2 and the location of ROI (240 pixels) around: x: 10 ; y: 989, non-projected. All data were downloaded and processed from MarsSI. The ratio column median from Bultel et al, 2015 applied on a portion of the image centred on Oxia clay deposits.

Library spectra are from RELAB; vermiculite (Spectra 5, 7 and 6; respectively VE-EAC-001; VE-EAC-002; VE-EAC-003) and Fe-Saponite (Spectrum 8; JB-JLB-F92-C).

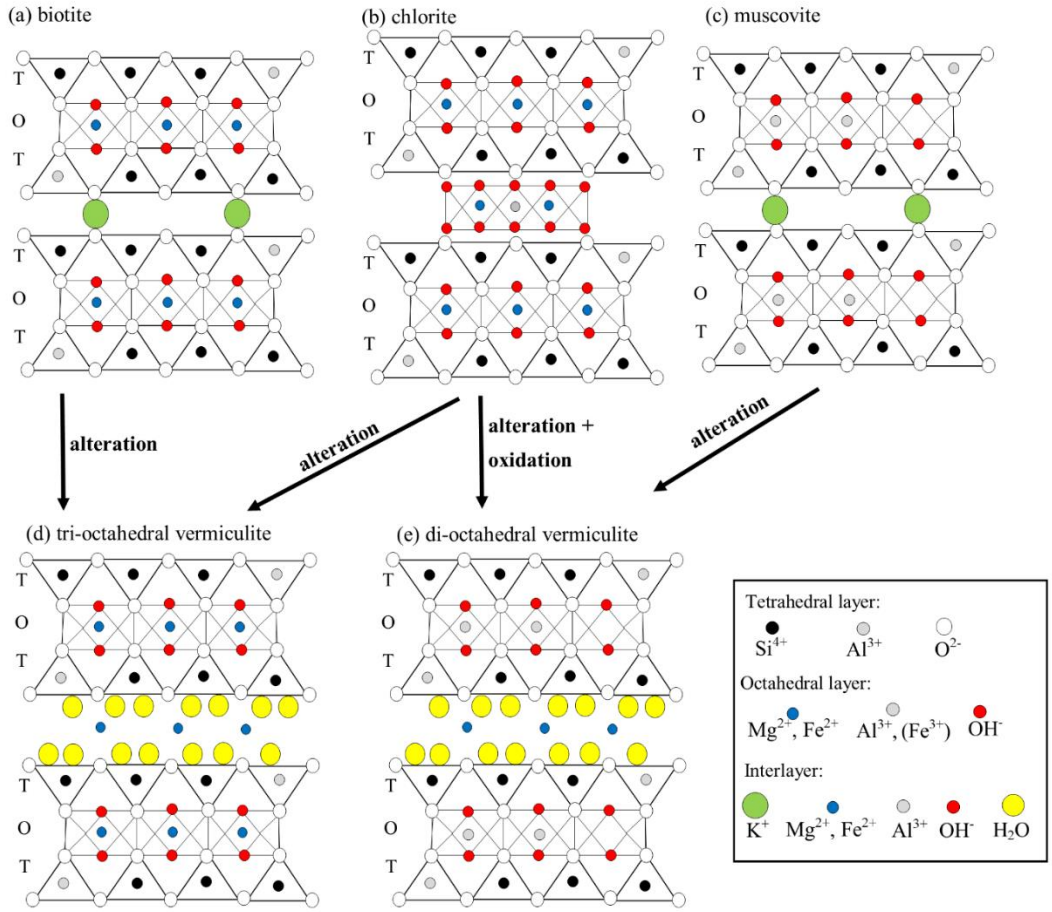


Fig. 2. Structure of vermiculite and primary phyllosilicates that can alter to vermiculite. TOT trioctahedral biotite has the largest potential to alter to trioctahedral vermiculite, whereas muscovite being dioctahedral, alters to dioctahedral vermiculite. In the case of chlorite, which is primary tricotahedral, weathering in anoxic conditions may lead to the formation of trioctahedral vermiculite. However, very commonly, oxidation accompanying alteration leads to transformation of the structure and formation of dioctahedral vermiculite.

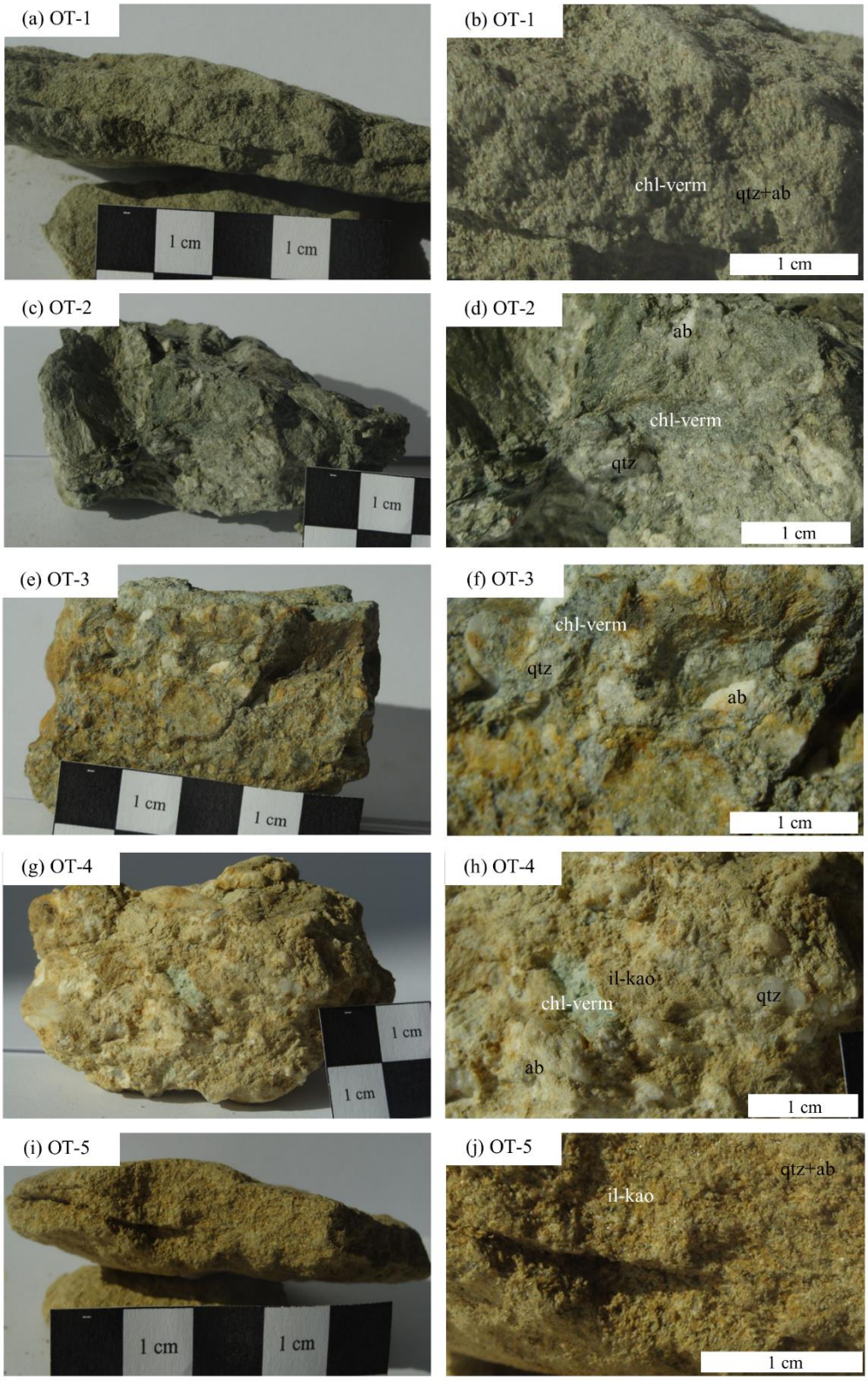


Fig. 3. Samples collected from Blue Spur Conglomerate deposits, Otago. (a-b and c-d) Greenish schists that contain vermiculite-smectite (chl-verm – vermiculite) clay. The colour suggests ferrous iron content in clays. (e-f) Most primary material with unaltered chlorite-rich clasts preserved. Detrital material with angular clasts of basement rock is seen (ab – albite, qtz – quartz). (g-h and i-j) Pale, oxidized rocks containing Al-phyllosilicates and/or Fe-oxides.

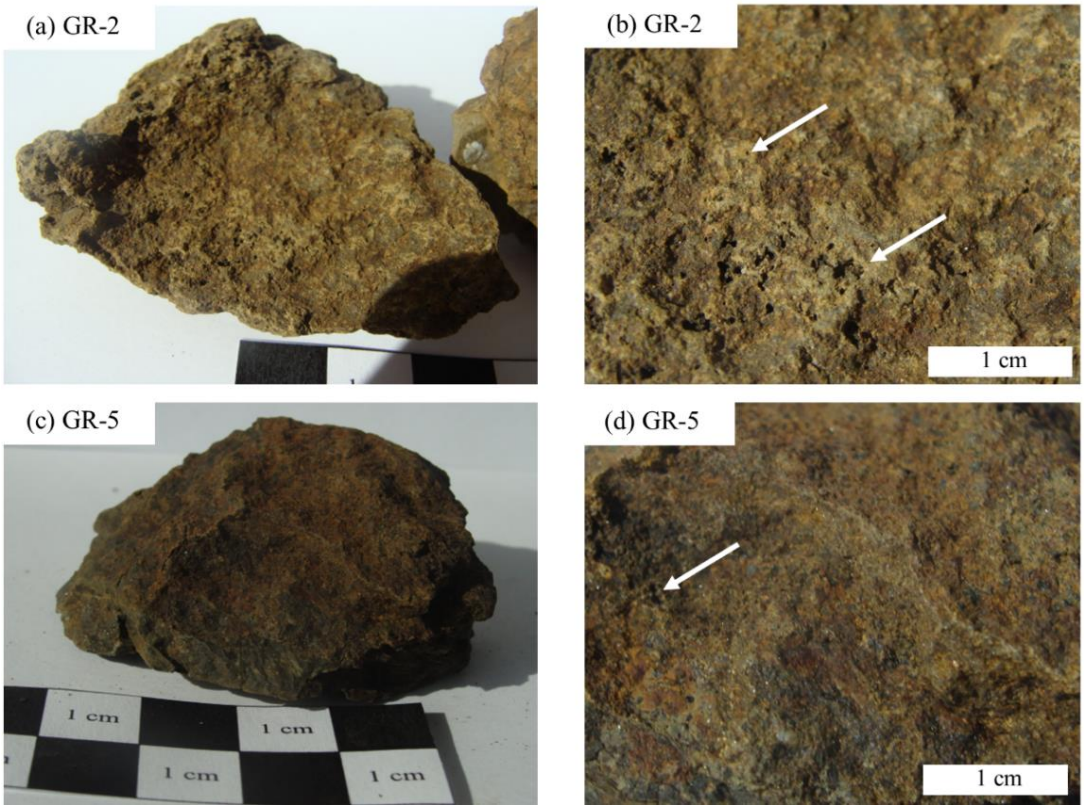


Fig. 4. Samples collected from Granby basaltic tuff formation. The basalts contain vesicles and amygdales (arrows) that are filled with phyllosilicates characterized previously (April and Keller, 1992) as vermiculite-saponite.

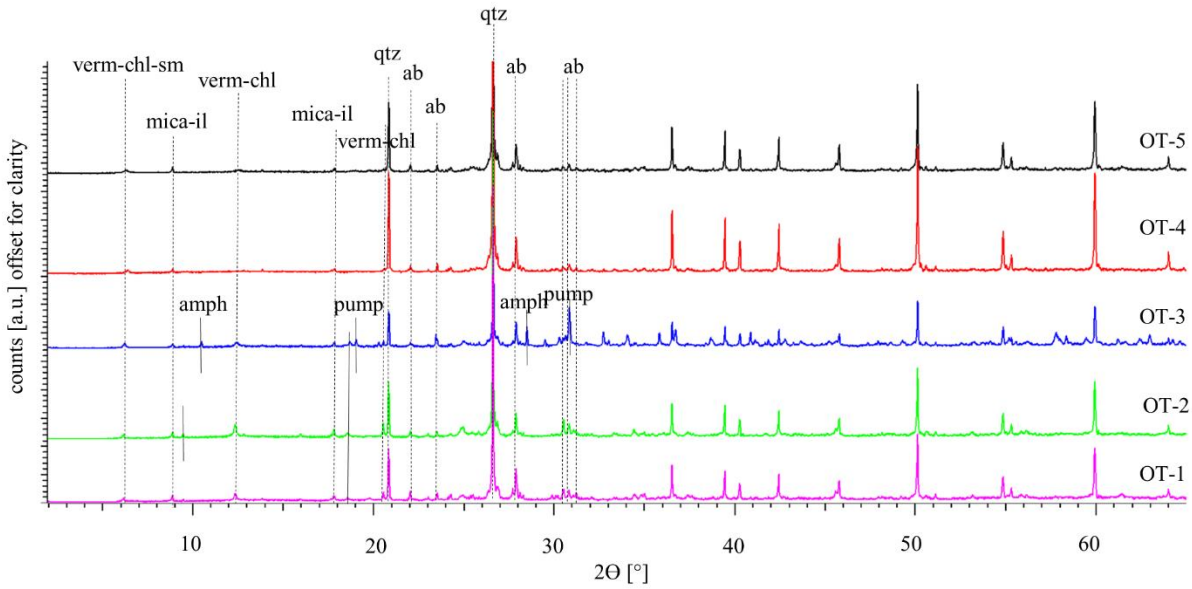


Fig 5. Bulk rock XRD patterns of samples collected from vermiculitized chlorite schists from Otago region. Peaks characteristic for main minerals present are marked: quartz (qtz), albite (ab), pumpellyite (pump), amphibole (amph). Clay minerals are present but cannot be identified from bulk patters: vermiculite-smectite and/or chlorite (verm-chl-sm) and mica and/or illite (mica-il).

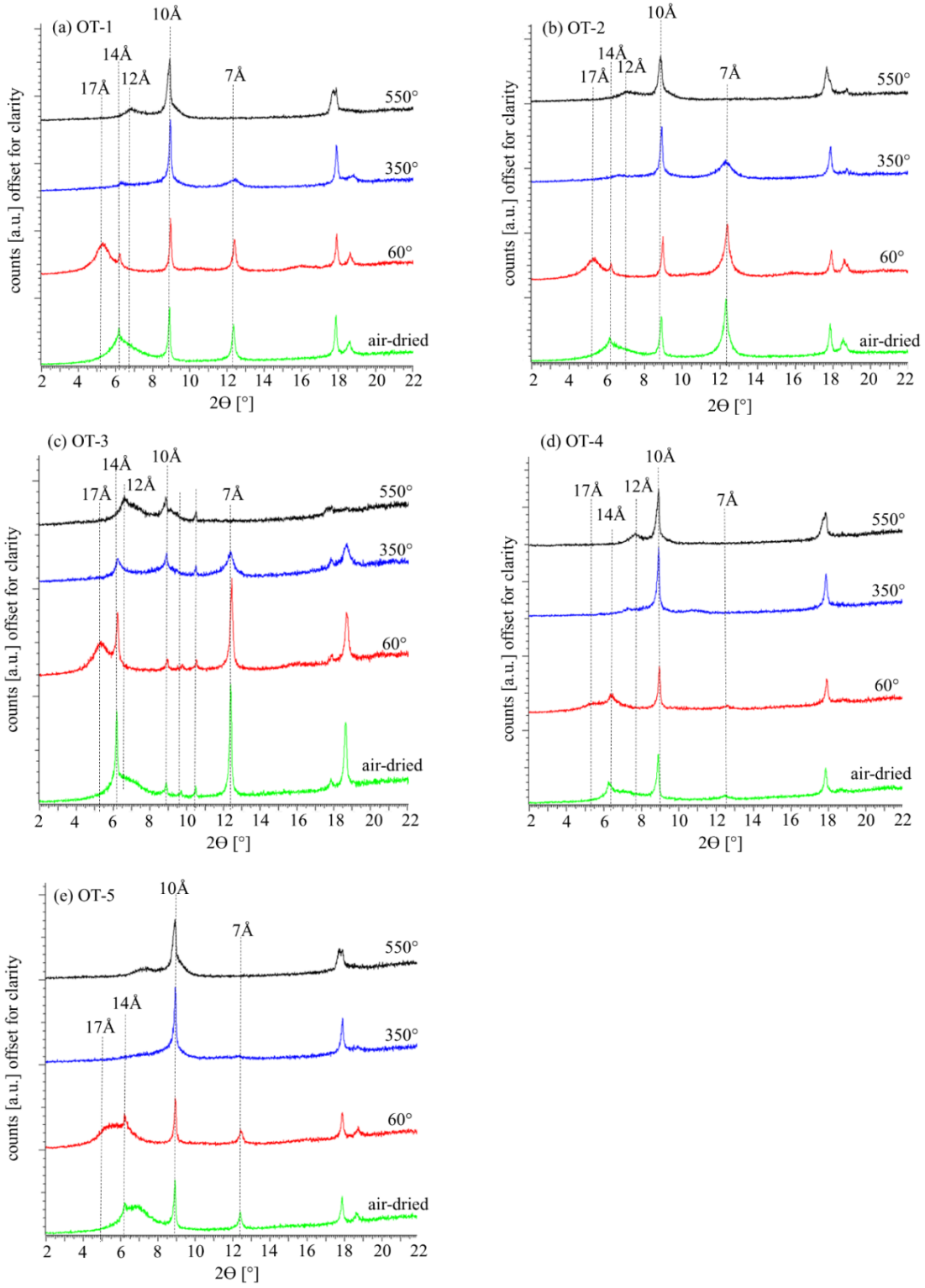


Fig. 6. XRD patterns of oriented clay fraction samples from Otago vermiculitized chlorite schists. Peak at 14Å shifting to 17Å at glycolation and collapsing to 10Å after heating suggest presence of expandable clay – vermiculite. Peak at 10Å that stays unchanged after treatment is characteristic of illite or illitized mica. Peak at 7Å, destroyed after heating is typical of chlorite. Broad shoulder at 10-14Å, shifting to higher d-spacing values under glycolation indicated interstratified vermiculite-illite.

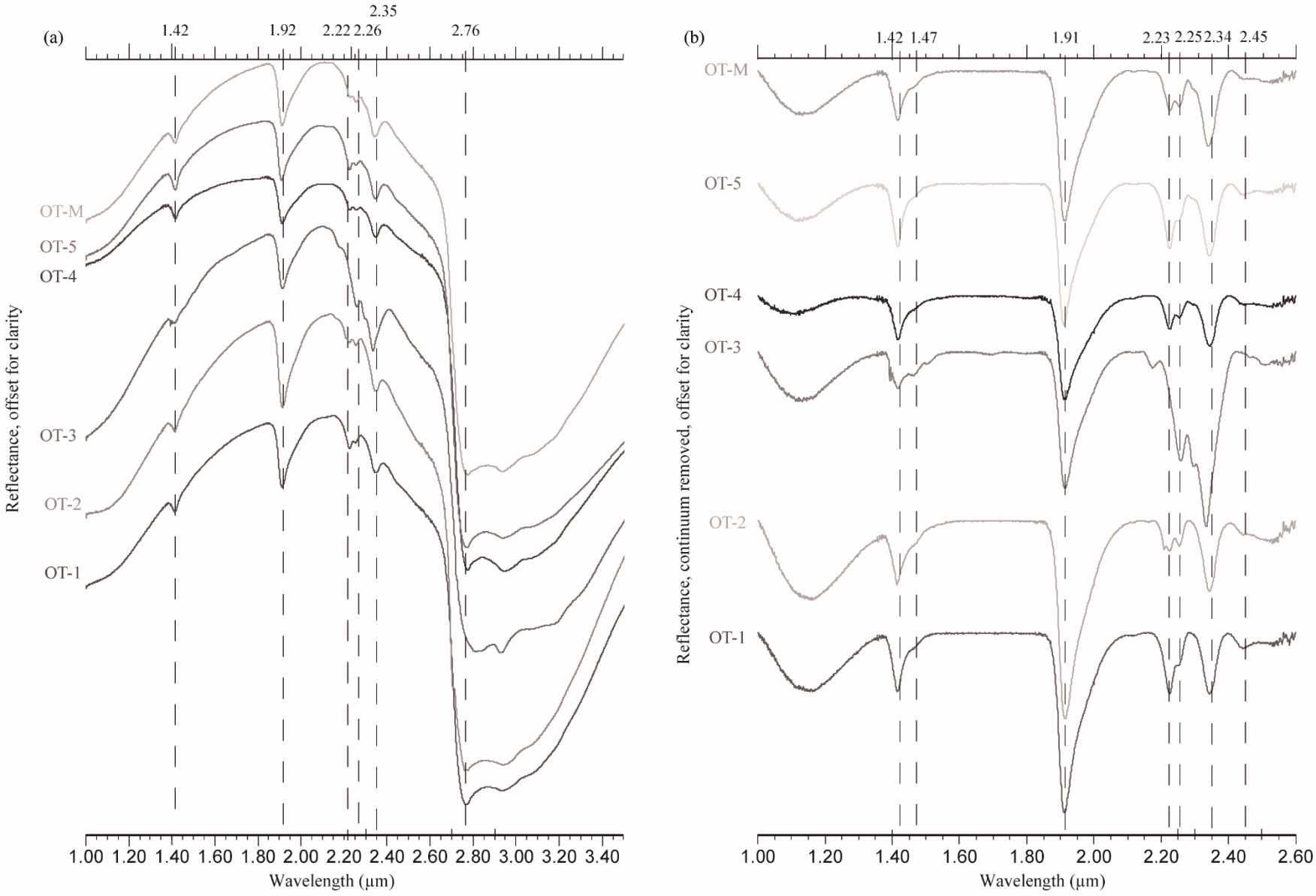
(a)
1.42
1.92
2.22
2.26
2.35
2.76
OT-M
OT-5
OT-4
OT-3
OT-2
OT-1
Reflectance, offset for clarity
1.00 1.20 1.40 1.60 1.80 2.00 2.20 2.40 2.60 2.80 3.00 3.20 3.40
Wavelength (μm)
(b)
1.42
1.47
1.91
2.23
2.25
2.34
2.45
OT-M
OT-5
OT-4
OT-3
OT-2
OT-1
Reflectance, continuum removed, offset for clarity
1.00 1.20 1.40 1.60 1.80 2.00 2.20 2.40 2.60
Wavelength (μm)

Fig. 7. NIR characterization of Otago samples (a) from 1.00 to 3.50 μm and (b) from 1.00 to 2.60 μm with continuum removed. (a) Characteristic absorptions at 1.42, 1.92, 2.22, 2.26, 2.35 and 2.75 μm are marked and their interpretation presented in table 3. (b) Absorptions at 1.42, 1.47, 1.91, 2.18, 2.23, 2.25, 2.34 and 2.45 μm are marked and interpreted in table 4.

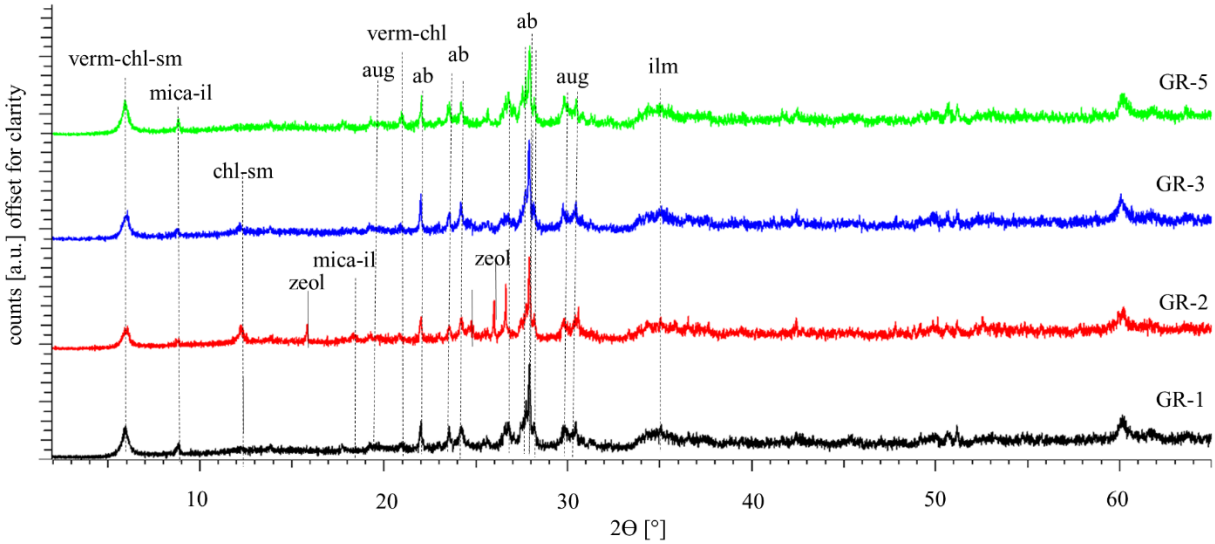


Fig. 8. Bulk rock XRD patterns of samples collected from clay-bearing Granby (GR-2 and GR-5) basaltic tuffs. Peaks characteristic for main minerals present are marked: albite (ab), augite (aug), ilmenite (ilm), zeolites (zeol). Clay minerals cannot be identified with certainty from bulk pattern, but presence of vermiculite-chlorite-smectite (verm-chl-sm) and mica-illite (mica-il) can be supposed.

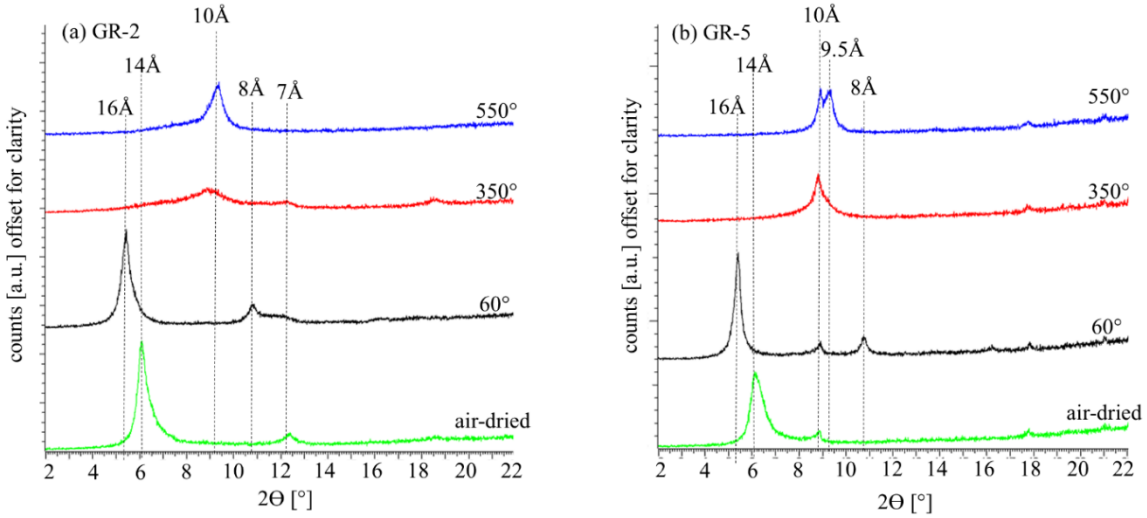


Fig. 9. XRD patterns of oriented clay fraction samples from Granby samples. Peak at 14Å shifting to 16Å at glycolation and collapsing to 10Å under heating suggest presence of expandable clay – vermiculite. The associated *00l* reflections at 7Å and 8Å suggest well crystallized nature of clay. Collapse to 10Å and 9.5 Å after heating indicates intergrowths of two expandable clays: likely vermiculite and saponite. Peak at 10Å (in b only) that stays unchanged after treatment is characteristic of mica, but full nature of clay is not reconstructed here.

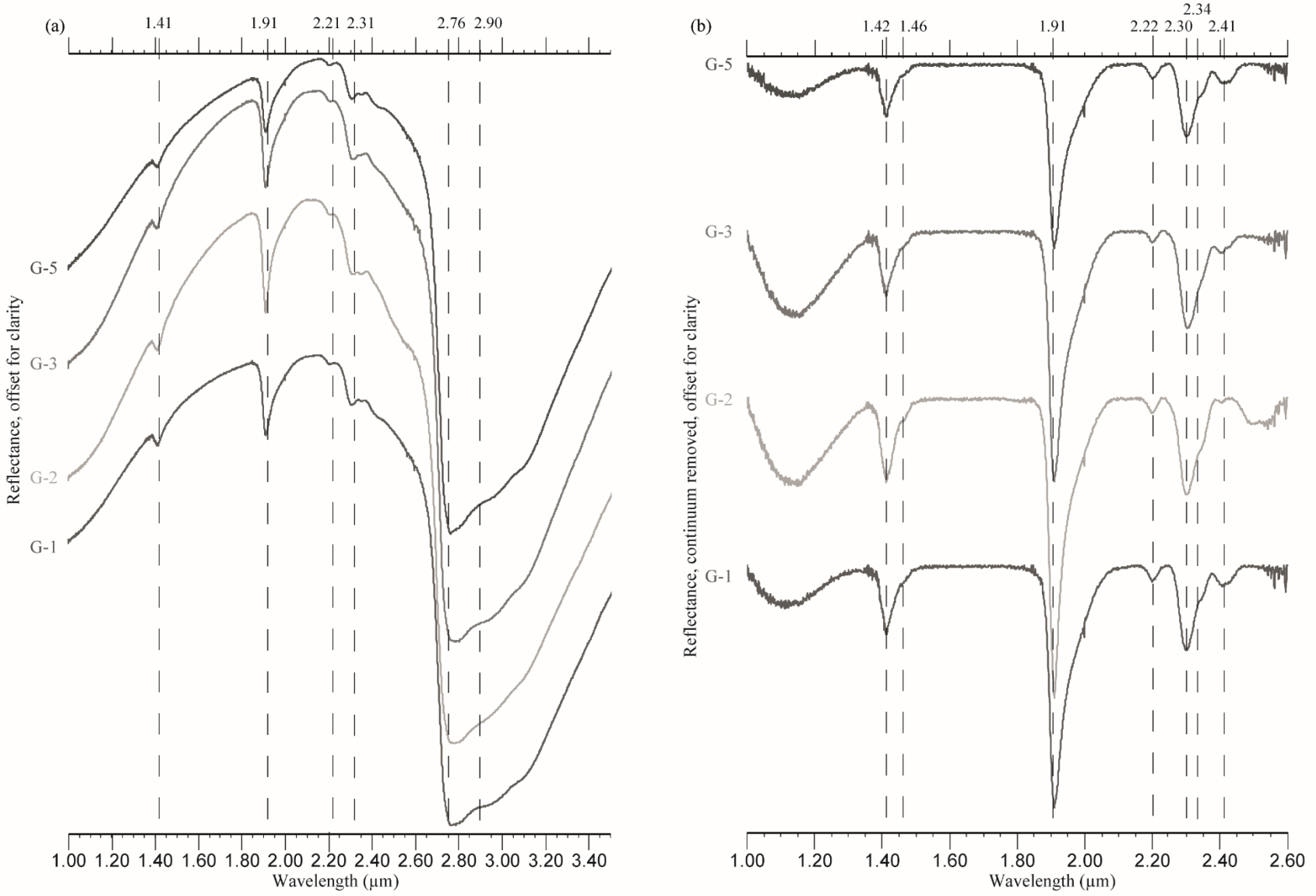
(a)
1.41
1.91
2.21 2.31
2.76 2.90
G-5
G-3
G-2
G-1
Reflectance, offset for clarity
1.00 1.20 1.40 1.60 1.80 2.00 2.20 2.40 2.60 2.80 3.00 3.20 3.40
Wavelength (μm)
(b)
1.42 1.46
1.91
2.22 2.30
2.34
2.41
G-5
G-3
G-2
G-1
Reflectance, continuum removed, offset for clarity
1.00 1.20 1.40 1.60 1.80 2.00 2.20 2.40 2.60
Wavelength (μm)

89

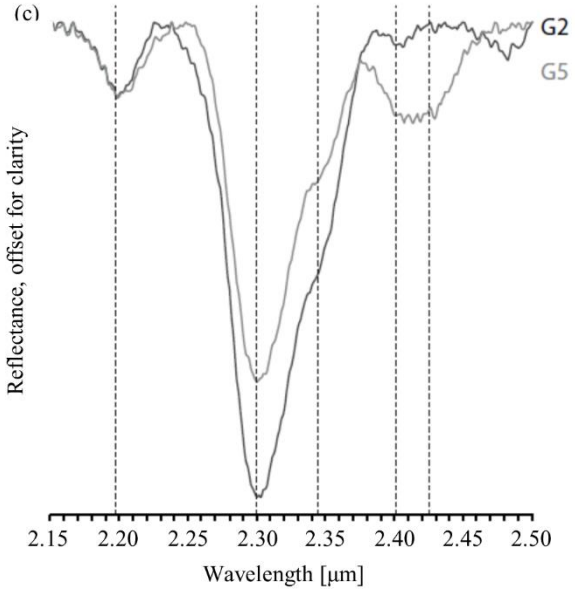


Fig. 10. NIR characterization of Granby samples (a) from 1.00 to 3.50 µm, (b) from 1.00 to 2.60 µm with continuum removed and (c) from 2.15 to 2.50 with continuum removed. (a) Characteristic absorptions at 1.41, 1.91, 2.21, 2.31, 2.76 and 2.90 µm are marked and their interpretation presented in table 7. (b) Absorptions at 1.42, 1.46, 1.91, 2.22, 2.30, 2.34 and 2.41 µm are marked and interpreted in table 8. (c) Absorptions at 2.20, 2.31, 2.35, 2.39 and 2.43 µm are best seen in continuum removed

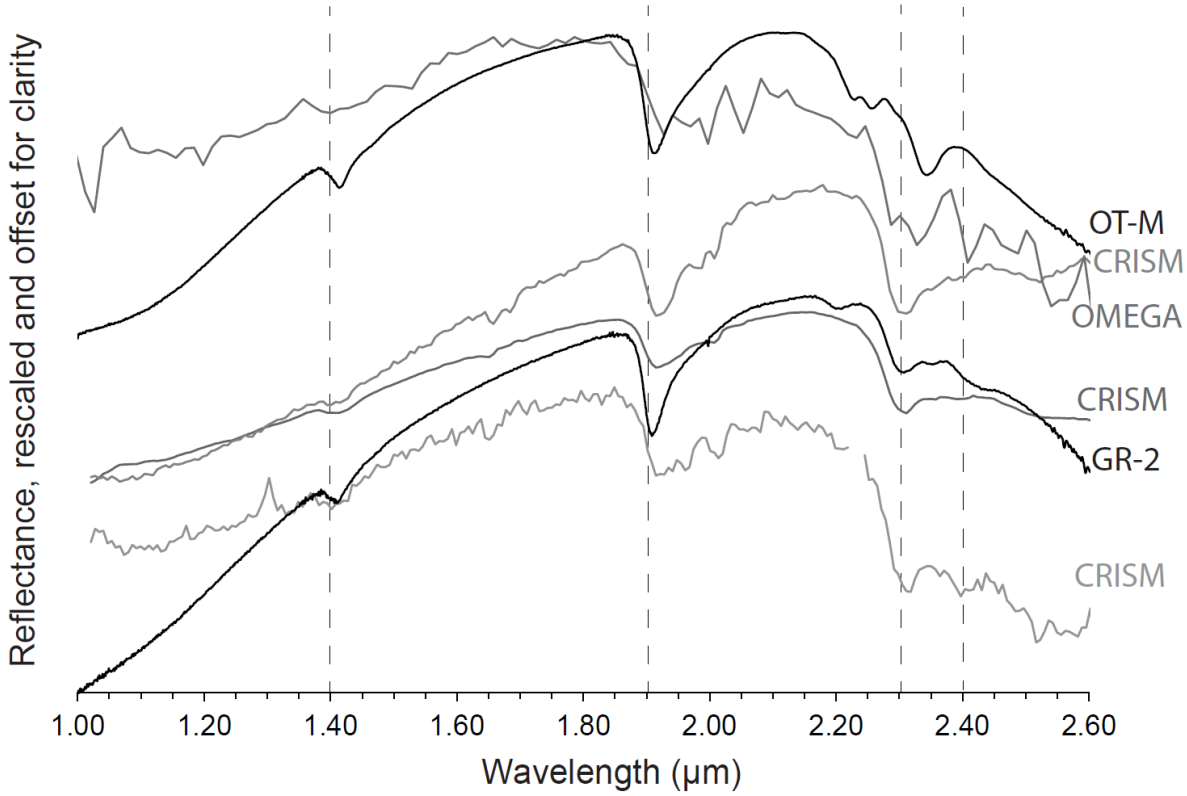


Fig. 11. Spectrum of Oxia Planum compared with spectrum of best identified analogue rock (GR-2, Granby 2) and spectrum of the other analogue (OT-M, Otago linear mixture). CRISM and OMEGA spectra are the same as shown in figure 1. For details of the spectrum G-2 refer to figure 10, for details of OT-M please refer to figure 7.

| Table 1. Position of each absorption centres (µm) in CRISM spectra of Oxia Planum. | | |
|---|---|---|
| Absorptions number | Oxia Planum | Interpretation |
| *1* | 1.00 | Crystal field transition for $Fe^{2+}$ (Hunt et al, 1977; Hunt & Salisbury, 1970) |
| *2* | 1.41-1.44 | O-H stretching and structural and absorbed $H_2O$ stretching (Clark et al, 1990) |
| *3* | 1.92 (vs) | O-H stretching and structural and absorbed $H_2O$ stretching (Clark et al, 1990) |
| *4* (revealed in OMEGA but not in CRISM) | 2.21-2.23 (w) | Al-OH stretching and bending (Clark et al, 1990; Chemtob et al, 2015) |
| *5* | 2.31-2.32 (vs) | Fe,Mg-OH stretching and bending, exact position depends on the Fe/Mg ratio and oxidation state of iron (King and Clark, 1989; Clark et al., 1990; Mustard et al., 1992; Chemtob et al., 2015, Michalski et al., 2015) |
| *6* | 2.38-2.41 (w ,*) | Fe,Mg-OH stretching and bending, exact position depends on the Fe/Mg ratio and oxidation state of iron (King and Clark, 1989; Clark et al., 1990; Mustard et al., 1992; Chemtob et al., 2015, Michalski et al., 2015) |
| *7* (identified by Mandon et al. 2021) | 2.50 (w) | Tentatively attributed to carbonates mixed with phyllosilicates (Mandon et al., 2021) |
| *8* | 2.90-2.95 | Absorbed $H_2O$ stretching and, possibly, Fe,Mg-OH stretching and bending (Clark et al, 1990) |
| w: weak, vs: very strong, *: strength variable across the area<br>For more quantitative interpretation of absorption strength, please refer to Figure 1. | | |

| Table 2. Summary of mineral composition of Otago samples, as revealed by bulk rock XRD analysis and clay fraction XRD treatment. | | | | | |
|---|---|---|---|---|---|
| Sample name / Mineral | OT-1 | OT-2 | OT-3 | OT-4 | OT-5 |
| quartz | + | + | + | + | + |
| plagioclase | + | + | + | + | + |
| hornblende | | | + | | |
| pumpellyite | | | + | | |
| vermiculite (trioctahedral) | + | + | minor | | |
| vermiculite (dioctahedral) or smectite | minor | minor | | + | + |
| interstratified vermiculite-illite | + | + | + | + | +++ |
| chlorite | + | + | +++ | minor | + |
| muscovite/biotite/illite | + | + | minor | +++ | +++ |

Table 3. Position of each absorption centres (µm) in NIR spectra of Otago samples with qualification of their strength in parenthesis.

| Sample name / Absorptions number | OT-1 | OT-2 | OT-3 | OT-4 | OT-5 | OT-Mix |
|---|---|---|---|---|---|---|
| *1* | 0.96 | 0.96 | 0.96 | 0.96 | 0.96 | 0.96 |
| *2* | 1.42 | 1.42 | 1.41 | 1.42 | 1.42 | 1.42 |
| *3* | 1.92 | 1.92 | 1.92 | 1.92 | 1.92 | 1.92 |
| *4* | 2.23 (s); 2.26 (w) | 2.22 (vw); 2.23 (w); 2.26 (s) | 2.19 (w); 2.26 (s) | 2.23 (w); 2.26 (w) | 2.23 (s); 2.26 (w) | 2.24 (w); 2.26 (s) |
| *5* | 2.35 (vs) | 2.35 (vs) | 2.31 (vw); 2.34 (vs) | 2.35 (vs) | 2.35 (vs) | 2.35 (vs) |
| *6* | vvw | vvw | vvw | vvw | vvw | vvw |
| *7* | 2.77 (vs) | 2.76-2.78 (dbl. vs) | 2.83 (vs) | 2.78 (vs) | 2.78 (vs) | 2.78 (vs) |

dbl: double; vvw: very very weak/knickpoint only; vw: very weak; w: weak; s: strong; vs: very strong.
For more quantitative interpretation of absorption strength, please refer to Figure 7a.

Table 4. Position of each absorption centres (µm) in NIR spectra of Otago samples with qualification of their strength in parenthesis. The continuum has been removed between 1.00 µm and 2.60 µm.

| Sample name / Absorptions number | OT-1 | OT-2 | OT-3 | OT-4 | OT-5 | OT-Mix |
|---|---|---|---|---|---|---|
| *2* | 1.42 (vs); 1.47 (vw); | 1.42 (vs); 1.47 (vw); | 1.42 (vs); 1.47 (w); 1.51 (w) | 1.42 (vs); 1.47 (vw); | 1.42 (vs); 1.47 (vw); | 1.42 (vs); 1.46 (vw) |
| *3* | 1.91 (vs) | 1.91 (vs) | 1.91 (vs) | 1.91 (vs) | 1.91 (vs) | 1.91 (vs) |
| *4* | 2.23 (s); 2.25 (vw) | 2.20 (vw); 2.22 (s); 2.26 (s) | 2.18 (w); 2.26 (vs) | 2.25 (s); 2.26 (w) | 2.23 (s); 2.26 (vw) | 2.23 (s); 2.25 (s) |
| *5* | 2.34 (vs) | 2.34 (vs) | 2.30 (vw); 2.33 (vs) | 2.34 (vs) | 2.34 (vs) | 2.34 (vs) |
| *6* | 2.44 (s) | 2.44 (s) | 2.47 (w) | 2.45 (s) | 2.45 (s) | 2.50 (w) |

vw: very weak, w: weak, s: strong, vs: very strong
For more quantitative interpretation of absorption strength, please refer to Figure 7b.

| Table 5. NIR spectra interpretation of Otago samples with an attempt to semi-quantify Fe, Mg or Al from absorptions 4, 5 and 6. | | | | | | |
|---|---|---|---|---|---|---|
| Sample name | OT-1 | OT-2 | OT-3 | OT-4 | OT-5 | OT-Mix |
| *4* | $AlFe^{3+}$ (+); $AlFe^{2+}$ (--) | Al (--); $AlFe^{3+}$(+); $AlFe^{2+}$ (+) | Al (-); $AlFe^{2+}$ (++) | $AlFe^{3+}$ (+); $AlFe^{2+}$ (-) | $AlFe^{3+}$ (+); $AlFe^{2+}$ (--) | $AlFe^{3+}$ (+); $AlFe^{2+}$ (+) |
| *5* | $Fe^{2+}$ (++) | $Fe^{2+}$ (++) | $Fe^{3+}$ (--); $Fe^{2+}$ (++) | $Fe^{2+}$ (++) | $Fe^{2+}$ (++) | $Fe^{2+}$ (++) |
| *6* | $Fe^{2+}$/Mg (+) | $Fe^{2+}$/Mg (+) | $Fe^{2+}$/Mg (-) | $Fe^{2+}$/Mg (+) | $Fe^{2+}$/Mg (+) | $Fe^{2+}$/Mg (-) |
| --, -, + and ++ indicate the relative strength of each cation's vibration from very low influence to very strong influence. | | | | | | |

| Table 6. Summary of mineral composition of Granby samples, as analysed by XRD. | | | | |
|---|---|---|---|---|
| Sample name / mineral | GR-1 | GR-2 | GR-3 | GR-5 |
| albite | + | + | + | + |
| augite | + | + | + | + |
| ilmenite | minor | minor | minor | minor |
| zeolite | | + | | |
| mica-illite | + | | minor | + |
| vermiculite (trioctahedral) | + | + | + | + |
| saponite | | minor | | + |

| Table 7. Position of each absorption centres (µm) in NIR spectra of Granby samples with qualification of their strength in parenthesis. | | | | |
|---|---|---|---|---|
| Sample name / Absor--ptions num--ber | GR-1 | GR-2 | GR-3 | GR-5 |
| *1* | 0.96 | 0.96 | 0.96 | 0.96 |
| *2* | 1.41 | 1.41 | 1.41 | 1.41 |
| *3* | 1.91 | 1.91 | 1.91 | 1.91 |
| *4* | 2.21 (w) | 2.21 (w) | 2.21 vw | 2.21 (w) |
| *5* | 2.31 (vs)<br>2.35 (w) | 2.31 (vs)<br>2.35 (w) | 2.32 vs<br>2.35 vw | 2.31 (vs)<br>2.35 (w) |
| *6* | vvw | vvw | vvw | vvw |
| *7* | 2.76 (vs) | 2.76 (vs) | 2.76 vs | 2.76 (vs) |
| dbl: double; vvw: very very weak/knickpoint only; vw: very weak; w: weak; s: strong; vs: very strong.<br>For more quantitative interpretation of absorption strength, please refer to Figure 10a. | | | | |

Table 8. Position of each absorption centres (µm) in NIR spectra of Granby samples with qualification of their strength in parenthesis. The continuum has been removed between 1.00 µm and 2.60 µm.

| Sample name / Absor--ptions num--ber | GR-1 | GR-2 | GR-3 | GR-5 |
|---|---|---|---|---|
| *2* | 1.42 (vs); 1.46 (vw); | 1.42 (vs); 1.46 (vw); | 1.42 (vs); 1.46 (vw); | 1.42 (vs); 1.46 (vw); |
| *3* | 1.91 (vs) | 1.91 (vs) | 1.91 (vs) | 1.91 (vs) |
| *4* | 2.22 s | 2.22 s | 2.22 s | 2.22 s |
| *5* | 2.30 (vs) 2.34 vvw | 2.30 vs 2.34 vvw | 2.31 vs | 2.30 vs 2.34 vvw |
| *6* | 2.41 (s) | 2.40 vw 2.51 s | 2.40 vw | 2.41 w |

vw: very weak, w: weak, s: strong, vs: very strong
For more quantitative interpretation of absorption strength, please refer to Figure 10b.

Table 9. NIR spectra interpretation of Granby samples with an attempt to semi-quantify Fe, Mg or Al from absorptions 4, 5 and 6.

| Sample name | GR-1 | GR-2 | GR-3 | GR-5 |
|---|---|---|---|---|
| *4* | Al3+ | Al3+ | Al3+ | Al3+ |
| *5* | Mg ++; Fe2+ | Mg ++; Fe2+ | Mg ++; | Mg ++; Fe2+ |
| *6* | Fe2+/Mg ++ | Fe2+/Mg + | Fe2+/Mg + | Fe2+/Mg ++ |

--, -, + and ++ denote the relative strength of each cation's vibration from very low influence to very strong influence